Oxalate metal complexes in aerosol particles: implications for the hygroscopicity of oxalate-containing particles

Takema Furukawa and Yoshio Takahashi

Department of Earth and Planetary Systems Science, Graduate School of Science, Hiroshima University, Higashi-Hiroshima, Hiroshima 739-8526, Japan
Received: 20 October 2010 – Accepted: 27 October 2010 – Published: 9 November 2010
Correspondence to: Y. Takahashi (ytakaha@hiroshima-u.ac.jp)

Abstract

Atmospheric aerosols have both a direct and an indirect cooling effect that influences the radiative balance at the Earth's surface. It has been estimated that the degree of cooling is large enough to weaken the warming effect of carbon dioxide. Among the cooling factors, secondary organic aerosols (SOA) play a key role in the solar radiation balance in the troposphere as SOA can act as cloud condensation nuclei (CCN) and extend the lifespan of clouds because of their high hygroscopic and water soluble nature. Oxalic acid is one of the major components of SOA, and is produced via several formation pathways in the atmosphere. However, it is not certain whether oxalic acid exists as free oxalic acid or as metal oxalate complexes in aerosols, although there is a marked difference in their solubility in water and their hygroscopicity. We employed X-ray absorption fine structure spectroscopy to characterize the calcium (Ca) and zinc (Zn) in aerosols collected at Tsukuba in Japan with fractionation based on particle size using an impactor aerosol sampler. It was shown that 10–60% and 20–100% of the total Ca and Zn in the finer particles (<2.1 μm) were present as Ca and Zn oxalate complexes, respectively. Oxalic acid is hygroscopic and can thus increase the CCN activity of aerosol particles, while complexes with various polyvalent metal ions such as Ca and Zn are not hygroscopic, which cannot contribute to the increase of the CCN activity of aerosols. Based on the concentration of noncomplexed and metal-complexed oxalate species, we found that most of the oxalic acid is present as metal oxalate complexes in the aerosols, suggesting that oxalic acid does not increase the hygroscopicity of aerosols in the atmosphere. Similar results are expected for other dicarboxylic acids, such as malonic and succinic acids. Thus, it is possible that the cooling effect of organic aerosols assumed in various climate modeling studies is overestimated because of the lack of information on metal oxalate and other dicarboxylic acid complexes in aerosols.

1 Introduction

Some anthropogenic aerosols, such as organic aerosols and sulfate aerosols, have a direct cooling effect by scattering solar radiation, and an indirect cooling effect by acting as cloud condensation nuclei (CCN) because of their hygroscopic properties (Novakov and Penner, 1993; Claeys et al., 2004; Kanakidou et al., 2005; IPCC, 2007; Hallquist et al., 2009). The global average contribution of the indirect cooling effect (i.e., the cloud albedo effect) is estimated to be −0.3 to −1.8W/m^2 (Charlson et al., 1992; IPCC, 2007). In the report of the Intergovernmental Panel on Climate Change (IPCC), the sum of the direct and indirect cooling effect of aerosols is almost equivalent to the warming effect of carbon dioxide (IPCC, 2007). However, a large uncertainty exists because of the indirect effect discussed in the IPCC report (2007), which must be evaluated more precisely for a better understanding of the Earth's climate. Thus, a number of studies have been performed on sulfate aerosols and on organic aerosols because of their complex nature in terms of composition and chemical transformation in the atmosphere, and also because of their importance in the global CCN budget (Novakov

and Penner, 1993; Claeys et al., 2004; Kanakidou et al., 2005; IPCC, 2007; Hallquist et al., 2009). Among the various organic aerosols studied, water-soluble organic compounds (WSOCs) in aerosols influence the heat budget at earth surface as they act as CCN activator because of their hygroscopic properties. In addition, we can assume that other dicarboxylic acids (DCA) also contribute to the CCN activity, considering that other DCA, which are major constituents of WSOCs, also have hygroscopic nature (Kawamura and Ikushima, 1993; Kawamura and Sakaguchi, 1999; Yao et al., 2002; Grahan et al., 2004; Lohmann and Leck, 2005; IPCC, 2007).

Oxalic acid is a major component of dicarboxylic acids or secondary organic aerosols (Kawamura and Ikushima, 1993; Kawamura and Sakagushi, 1999; Yu, 2000). In this study, we focused on oxalic acid as a representative component of low molecular weight dicarboxylic acids in the atmosphere, and our results can be extended to other DCA, such as malonic and succinic acids. Oxalic acid can form metal oxalate complexes in aerosols by reacting with metal ions because: (i) aerosols contain various metal ions originating from sea salts, desert dusts, continental soils, and anthropogenic sources; (ii) oxalic acid is formed in the aqueous phase at aerosol surfaces in the atmosphere, which provides a reaction field for metal complexation; and (iii) polyvalent metal ions can form stable complexes with oxalate ions (Warneck, 2003; Grahan et al., 2004; Lim et al., 2005; Carlton et al., 2007; Ervens and Volkamer, 2010). However, metal oxalate complexes are not detected using conventional methods, such as gas chromatography and ion chromatography (IC). In the latter analysis, a large volume of water sufficient to dissolve metal oxalate complexes in aerosols is usually employed during the water extraction procedure. In this case, metal oxalate complexes can be readily dissolved, despite the low solubility of some metal oxalate complexes (for more details, see Sect. 3.5), and it is difficult to distinguish between noncomplexed and metal-complexed oxalate species in aerosols. Hence, only a few studies have suggested that WSOCs can react with metal ions and mineral aerosols (Mochida et al., 2003, 2007; Sullivan et al., 2007). However, these studies employed indirect methods that cannot show any direct evidence of the formation of metal oxalate complexes in aerosols.

In this study, we applied X-ray absorption fine structure (XAFS) spectroscopy to show the presence of metal oxalate complexes in aerosols, coupled with IC and inductively coupled plasma atomic emission spectrometry (ICP-AES) analyses to determine the ratio of metal oxalate and noncomplexed oxalate species. XAFS data consists of X-ray absorption near edge structure (XANES) and extended X-ray absorption fine structure (EXAFS), which enables us to determine chemical species of each element in aerosols directly (e.g., Takahashi et al., 2006; Higashi and Takahashi, 2009). In the XAFS analysis, size-fractionated aerosol samples were collected during 2002 in the winter (from January to February) and summer (from July to August) in Tsukuba, Japan. Based on our results, it was possible to obtain the ratio of metal-complexed and noncomplexed oxalate species in the aerosols. In this study, Ca K-edge XANES and Zn K-edge XANES and EXAFS were performed to demonstrate the presence of metal oxalate complexes. The ratio determined in this study can contribute to the precise evaluation of the influence of oxalic acid and other DCA on the hygroscopicity and CCN activity of aerosol particles.

2 Materials and methods

2.1 Aerosol samples and characterization

The aerosol samples examined in this study were collected in Tsukuba (a city approximately 60 km northeast of Tokyo: 36.06°N, 140.14°E) in Japan during the winter (21 January to 12 February) and summer (28 July to 13 August) of 2002 (Kanai et al., 2003) as a part of the Japan–China joint "Asian Dust Experiment on Climate Impact" project (Mikami et al., 2006). In this study, size-fractionated aerosol samples were collected using a low-volume

Andersen-type air sampler (AN-200, Shibata, Tokyo). The flow rate of the sampler was stabilized at 28.3 $Lmin^{-1}$ to achieve the ideal size separation of the aerosols. The sampler had eight stages and a back-up filter. The particle diameter was classified by the aerodynamic diameter as follows: >11.0 μm (sampling Stage 0), 11.0–7.0 μm (Stage 1), 7.0–4.7μm (Stage 2), 4.7–3.3 μm (Stage 3), 2.1–3.3 μm (Stage 4), 2.1–1.1 μm (Stage 5), 1.1–0.65 μm (Stage 6), 0.65–0.43 μm (Stage 7), and <0.43 μm (back-up filter). The filters used for Stages 0–6 were Advantec PF050 polyflon filters (diameter=80 mm; Advantec, Tokyo, Japan). A polyflon filter was used because these filters do not contain any major elements nor do they react with any acid gases during sampling. The filters used for Stage 7 and the back-up filters were Tokyo Dylec 2500QAT-UP quartz filters (Tokyo Dylec, Tokyo, Japan). The filters were weighed before and after sampling with a reading precision of 10 μg after stabilizing the weight under constant humidity in a desiccator. A sample mass >1mg was preferable when measuring the sample weight using a microbalance, and thus, the sampling period depended on the aerosol concentration in the atmosphere. Three-dimensional air mass back trajectories were calculated at 1000 m height using the Hybrid Single-Particle Lagrangian-Integrated Trajectory (HYSPLIT4) model (Draxler and Rolph, 2003).

2.2 Water soluble components in the aerosol samples

Bulk chemical analysis of the water soluble components (WSCs) in the aerosol was conducted using the procedure used by Kanai et al. (2005). A 1/8 section of the filter was soaked in a Teflon beaker containing 200 μL of ethanol and 5 mL of MQ water. The WSCs were leached by subjecting the solution to an ultrasonic treatment for a period of 30 min. The water soluble fraction was then recovered as a filtrate after filtration through a 0.20 μm hydrophilic polytetrafluoroethylene filter. The solution containing various extracted ions was used to determine the quantity of major anions (Cl^-, NO_3^-, SO_4^{2-}, and $C_2O_4^{2-}$) and cations (Na^+, NH_4^+, and K^+). The WSCs were measured using IC (IC7000, Yokogawa, Japan, relative precision =2%) employing Shodex IC YK-421 and Shima-pack IC-SA1/-SA1(G) columns for the cations and anions, respectively. The eluent composition was a mixed solution containing 24 mM of boric acid, 5 mM of tartaric acid, and 1 mM of 2,6-pyridine dicarboxylic acid for the cations and 14 mM of $NaHCO_3$ for the anions. The flow rate of the elutant was 1.0 $mLmin^{-1}$ for both cations and anions. A part of the extraction solution was used to determine the concentration of the water soluble fraction of Zn^{2+}, Ca^{2+}, and Mg^{2+} using ICP-AES (SEIKO EG&G, SP 500).

2.3 XAFS measurements

Calcium (Ca) K-edge XANES experiments were performed at Beamline 9A (Takahashi et al., 2006, 2009) at the KEK Photon Factory in Tsukuba, Japan. Beamline 9A has Si (111) double-crystal monochromators. The beam size was smaller than 1×0.5 mm^2 at the sample position. The aerosol samples located on each filter appeared as a dark spot (spot size= 0.5–2 mm), and were directly exposed to the incident X-ray beam. The entire beam path of Beamline 9A was filled with He gas to suppress any X-ray absorption and scattering from air. The energy of the Ca K-edge XANES was calibrated by defining the peak maximum of the XANES data of $CaCl_2 \cdot 2H_2O$ at 4038.1 eV. For the aerosol samples, fluorescence yield (FL) mode was employed to record the Ca K-edge XANES spectra. The CEY mode was used to obtain XAFS for reference materials, since the mode is not affected by overabsorption effect for concentrated sample (Manceau et al., 2002; Takahashi et al., 2009). The FL-XANES data were measured mainly for aerosol samples using a Lytle detector or a 19-element Ge solid state detector, since the mode is more sensitive that can be applied to natural samples. We confirmed that the two modes gave identical spectra when the samples were prepared appropriately to each mode (Takahashi et al., 2008, 2009). In the FL mode, the sample was placed at an angle of

45° to the incident beam. The Ca K-edge XANES spectra were recorded using a step size of 0.25 eV and a count per step of 0.5 s.

The zinc (Zn) K-edge XANES and EXAFS data were measured at Beamline 12C at the KEK-PF in Tsukuba, Japan. Beamline 12C also had a Si (111) double-crystal monochromator and the beam size <1×0.5 mm^2 at the sample position. The energy of the Zn K-edge XANES was calibrated by defining the peak maximum of Zn metal foil at 9660.7 eV. The transmission and FL modes were employed to measure the Zn K-edge XANES and EXAFS data of the reference materials and samples. In the FL mode, the aerosol sample was placed at an angle of 45° from the incident beam, and the fluorescent X-rays were measured using a 19-element Ge solid state detector. Supplementary data for Zn K-edge XAFS were also obtained at Beamline BL01B1 in SPring-8 (Hyogo, Japan), which has a similar set-up to that of Beamline 12C in Photon Factory.

The fitting of the spectra of natural samples to those of the reference materials was conducted using a least-squares fitting method. To estimate the goodness-of-fit in fitting the XANES and EXAFS spectra, the *R* value in the energy region for the fitting was

$$R = \sum (I_s(E) - I_{cal}(E))^2 / \sum I_{cal}(E)^2$$

where I_s and I_{cal} are the normalized absorption of the aerosol samples and the calculated values, respectively. The energy range for fitting the Ca K-edge XANES was 4030–4060 eV for Stages 5–7, while for the Zn K-edge XANES the energy range was 9650–9680 eV. The fitted range of the Zn K-edge EXAFS was from $\boldsymbol{k}$ = 2 to $\boldsymbol{k}$ = 6–7.5 $Å^{-1}$, where $\boldsymbol{k}$ is the photoelectron wave vector. The error for each fraction of the end members obtained from the XANES fitting was calculated using the Athena XAFS analysis software package (Ravel and Newville, 2005).

All the Ca and Zn standard materials used for fitting the spectra in this study were of analytical grade, and were obtained from Wako Pure Chemical Industries Ltd. (Osaka, Japan) or the Kanto Chemical Co. Inc. (Tokyo, Japan).

3 Results and discussion

3.1 Characterization of the aerosol samples

The results of backward trajectory (HYSPLIT4) analysis suggested that the air mass in winter in Tsukuba was transported through northeastern China, Korea, and Japan possibly subject to the influences of (i) anthropogenic aerosols from the mega cities in the three countries, (ii) mineral aerosols from arid area in northeast part of China (Mikami et al., 2006), and (iii) sea salts from Japan Sea (Fig. S1). In summer, the air mass mainly came from Pacific Ocean, but can also be affected by anthropogenic aerosols from industrial area in Japan, since the trajectory passed through Tokyo and Osaka. The seasonal trend is a typical for the air mass around Japan, and the chemical composition of the aerosols reflects the source of the air mass (Var et al., 2000).

Two peaks in the aerosol mass distribution were observed in the fine (particle size around 0.7 μm) and coarse (2–6 μm) modes in both winter and summer (Fig. 1). Most of the aerosols with finer fractions (<2 μm) may be secondary aerosols from anthropogenic sources. These aerosols were formed by the conversion from the gas phase to particles to form agglomerates of smaller sized particles (Seinfeld and Pandis, 2006). On the other hand, the coarse fraction mainly consisted of mineral aerosols transported from continental deserts, soil components, and sea salts (Seinfeld and Pandis, 2006).

The size-segregated chemical compositions also reflect the sources. Briefly, relative composition of sulfate to Na^+ showed that more than 95% of sulfate is of non-sea salt origin (nss-sulfate; Table S1), most of which should be anthropogenic. The concentration of nss-sulfate was calculated as (e.g., Uematsu et al., 2010)

$$[\text{nss-}SO_4^{2-}] = [\text{total } SO_4^{2-}]_{aerosol} - ([SO_4^{2-}]/[Na^+])_{seawater} \times [Na^+]_{aerosol}$$

where molar ratio of $([SO_4^{2-}]/[Na^+])_{seawater}$ was 0.051 (Bruland and Lohan, 2003). Thus, the aerosols samples in the both periods are affected largely by anthropogenic activities. The concentration of Na^+ in summer was approximately three times larger than that in winter, suggesting that aerosol samples in summer was affected by Pacific Ocean to a larger degree than in winter. These results agreed well with the back trajectory analysis (Fig. S1).

3.2 Size distribution of the WSCs in the aerosols

The formation of oxalate in the aerosols can be deduced from the chemical composition of the WSCs of the size-fractionated samples (Fig. 1 and Table S2) (Yao et al., 2002). The size distribution of oxalate is usually similar to that of sulfate, as the in-cloud process is important for the formation of both oxalate and nss-sulfate (Yao et al., 2002; Warneck, 2003). The peak in sulfate concentration occurs at 0.8 μm in both winter and summer, whereas the concentration of sulfate is higher in summer than in winter (Figs. 2 and 3). It is well established that the peak in sulfate particle size is formed by an in-cloud process noted as droplet mode (Yao et al., 2002; Seinfeld and Pandis, 2006). Similarly, ammonium in both seasons is formed in the droplet mode (Figs. 2 and 3). These results suggest that most of the sulfate is in the form of the ammonium salt in the finer particles, which is evident in the sulfur K-edge XANES data for the samples taken at Tsukuba (Takahashi et al., 2006).

In the oxalate size distribution, however, the peak is shifted towards coarser particle size than that of sulfate in summer (Figs. 2 and 3). A similar shift has also been observed by Yao et al. (2002) and Mochida et al. (2003, 2007). Oxalate in aerosols can be formed by several mechanisms: (i) oxalic acid particles can be captured in preexisting aerosols, such as sulfate aerosols, after the formation of an oxalate aerosol in the gas to particle conversion process (condensation mode); (ii) oxalate species can be formed in in-cloud processes; (iii) oxalate can form in the aqueous phase at the surface of the aerosol particles. In these processes, photooxidation is important that can produce oxalate from its precursors such as unsaturated hydrocarbons and volatile organic compounds (VOCs) with OH radical or O_3 (e.g., Satsumabayashi et al., 1990; Sullivan and Prather, 2007). Among the three processes, the process (i) cannot explain the high concentration observed around a particle size of 1.6 μm that shifted towards coarser particle size only in the summer, because the maximum surface area of the (secondary) aerosols had a particle size <1 μm (Seinfeld and Pandis, 2006). The second and third processes can explain the shift towards a coarser particle size by: (a) evaporation of oxalic acid in the finer particle sizes, which would result in an increase in the relative amount of oxalate in the coarser particles (Yao et al., 2002); and (b) a heterogeneous reaction of oxalic acid with coarser particles, such as mineral dusts (Yao et al., 2002; Mochida et al., 2003; Mochida et al., 2007, Russell et al., 2002; Sullivan and Prather, 2007), particularly if it is alkaline aerosols. Further discussion regarding the shift in particle size will be given in Sec. 3.6.

The size distribution of Cl^- and NO_3^- was similar in each period (Figs. 2 and 3), and the correlation coefficient between Cl^- and NO_3^- for various particles in each period was high (Table S3). Moreover, the size distribution of these ions was different between winter and summer. The peak in Cl^- and NO_3^- was found in the finer particle size in winter, but larger size in summer. Thus, Cl^- in the coarser mode in summer reflects the composition of sea salts (NaCl), while NO_3^- resulted from the uptake of HNO_3 gas by NaCl particle with water shell (Zhuang, 1999). Consequently, their correlation coefficient (R^2) was very high (> 0.9). This result is also consistent with the backward trajectory analysis (Fig. S1).

On the other hand, distribution of these ions into finer particles resulted from the gas to particle conversion of NH_4Cl and NH_4NO_3, respectively (Seinfeld and Pandis 2006),

NH_3 (gas) + HCl (gas) → NH_4Cl (particle)

NH_3 (gas) + HNO_3 (gas) → NH_4NO_3 (particle)

These chemical reactions depend on the surrounding environment, because Cl^- and NO_3^- ions in

the aerosols are likely to be affected by the ambient conditions, such as the RH (%), temperature, and photochemical factor (Oum et al., 1998; Zhuang et al., 1999; Yao et al., 2003; Seinfeld and Pandis, 2006; Thornton et al., 2010). Moreover, the origins of HCl (gas) and HNO_3 (gas) are mainly anthropogenic (Kaneyasu et al., 1999; Seinfeld and Pandis, 2006), showing that anthropogenic air masses affected the composition of aerosols in Tsukuba during winter in our samples.

A peak in the size distribution of Ca^{2+} and Mg^{2+} ions was observed in the coarser particle size in each period (Figs. 2 and 3), suggesting that the source of these ions was mainly natural, such as mineral dust from soil and arid areas and sea salt particles (Seinfeld and Pandis, 2006). The correlation coefficient of Ca^{2+} and Mg^{2+} ions with Na^{+} was relatively high (Table S2). However, the enrichment factor normalized by sea salt (EF_{ss}) for Ca^{2+} suggested that its source was not only sea salt but also from other sources such as soil particles. In contrast, EE_{ss} of Mg^{2+} is around or under 1, which is lower than that of Ca^{2+}, suggesting that sources of Mg^{2+} was mainly sea salt (Fig.S2).

Tsukuba was affected by anthropogenic air mass in both seasons (Fig. S1). Zinc ion is included in anthropogenic aerosols (Kauppinen and Pakkanen, 1990; Manoli et al., 2002; Adachi and Tainosho, 2004; Councell et al., 2004; Rauch and Pacyna, 2009), and has an important role on the formation of metal oxalate complexes due to its high stability constant with oxalate.

Among various heavy metals (Co, Ni, Zn, Mo, and Cd), concentration of Zn was larger than the other metals by more than an order of magnitude in the aerosols collected in Tsukuba (Ohta et al., 2003). The size distribution of Zn^{2+} ions was similar to the total oxalate distribution (Fig. 4). The peak in the size distribution of Zn^{2+} ions in the aerosols was found in the droplet mode in both periods. Hence, the source of Zn^{2+} ions in the aerosols can be mainly anthropogenic, such as from the exhausts of motor vehicles, tire wear, brake wear, biomass burning, coal burning, and incineration (Kauppinen and Pakkanen, 1990; Manoli et al., 2002; Adachi and Tainosho, 2004; Councell et al., 2004; Moffet et al., 2008; Rauch and Pacyna, 2009).

3.3 Ca oxalate in the finer particles

XAFS measurements at the Ca K-edge were carried out to demonstrate the presence of Ca oxalate ($CaC_2O_4 \cdot H_2O$) complexes in the aerosols. From their stability constants, Ca ions are the dominant divalent metal ion in aerosols that can form stable oxalate complexes (Table 1). Figure 5 shows the spectra of aerosol samples and Ca species used to fit the sample spectra. The fractions of Ca species obtained from the fitting are shown in Table 2, and the results of the XANES spectra of various Ca species are shown in Fig. S3. Based on these results, it is suggested that Ca oxalate was observed in the finer particles as 0.43–2.1 μm and 0.65–2.1 μm during the winter and the summer, respectively. The XANES fitting showed that the Ca oxalate fraction among the total Ca concentration was 10–60% (Fig. 5 and Table 2). The peak in the size distribution of the total oxalate occurred in this particle size range, where Ca oxalate is the main Ca species. In this range, the molar concentration of Ca^{2+} ion was lower than that of the total oxalate concentration, supporting the presence of Ca oxalate in this particle size.

Gypsum ($CaSO_4 \cdot 2H_2O$) and Ca nitrate ($Ca(NO_3)_2 \cdot 2H_2O$) were also observed in the same particle size range, and the XANES spectrum of Ca oxalate was similar to that of gypsum and Ca nitrate (Fig. S3). Assuming that gypsum and Ca nitrate were the end members of Ca in the aerosols in the fitting, then the sample spectra could not be fit, especially around 4047 eV (Fig. S4). On the other hand, the spectra could be fitted perfectly, even around 4047 eV, by assuming that Ca oxalate was one of main Ca species (Fig. S3). This result confirms that Ca oxalate is the main Ca species in the finer particles.

In the coarser particles (>2.1 μm), the Ca species determined from the fitting were calcite ($CaCO_3$), gypsum ($CaSO_4 \cdot 2H_2O$), and anhydrite ($CaSO_4$) in both periods (Fig. S3 and Table 2).

However, the XANES spectra of the finer particles could not be fitted using these three components (Fig. S4). This result also suggested the presence of Ca oxalate in the finer particles. Gypsum and anhydrite can be formed from sea salt particles or from a reaction of calcite and SO_x gas at the particle surface in the atmosphere (Buseck and Pósfai, 1999; Takahashi et al., 2009). Calcium nitrate can be formed from the reaction of calcite and NO_x gas (Krueger et al., 2003; Li and Shao, 2009).

Sullivan et al. (2009) suggested that the hygroscopicity and CCN activation property of oxalic acid can be reduced by reacting with Ca^{2+} in aerosols. Generally speaking, chemical species with low water solubilities are not hygroscopic, which results in the low CCN activity. Thus, Ca oxalate has low hygroscopicity and CCN activity due to the low solubility (0.617 mg/100g; Table 1). Similar characteristics can be extended to other metal oxalate complexes such as Zn and lead (Pb) oxalate due to their low water solubilities (Table 1). Formation of Zn and Pb complexes can be important considering their high abundances in anthropogenic aerosol particles (Espinosa et al., 2001; Manoli et al., 2002; Hao et al., 2007). To quantify the role of oxalic acid on the CCN activity of aerosol particles, the ratio of oxalic acid and total metal oxalate complexes such as Ca oxalate is important, which will be determined in Sec. 3.5 in this study.

3.4 Zn oxalate in the finer particles

Although the formation of Ca oxalate was suggested in the previous section, it is still necessary to confirm the results using independent data from other metal ions. Among the various divalent cations that can form stable complexes with oxalate (Table 1), Zn K-edge XAFS data was examined to show the formation of Zn oxalate, or other metal oxalate complexes, because: (i) Zn is the second most abundant divalent cation in the aerosol samples, and (ii) the stability constant of Zn oxalate is large and its water solubility is low (Table 1). In addition, (a) for other cations such as Pb and copper (Cu), it was not possible to obtain good quality spectra for the speciation analysis due to their low concentrations and (b) our system using hard X-ray cannot be applied to Mg. Thus, we confined our XAFS measurements to Ca and Zn

The Zn species in the aerosols at Tsukuba during the winter and summer were measured using Zn K-edge XANES and EXAFS spectra. Various XANES and EXAFS spectra of standard materials for Zn are shown in Fig. S5. The XANES spectra were obtained for particle sizes of these samples (Fig. 7), while EXAFS spectra were obtained only for the finer particle sizes (Fig. 8) where the Zn concentration was high, since high concentration is essential to obtain high quality EXAFS spectra. Based on the fitting of the XANES spectra (Table 3), Zn oxalate ($ZnC_2O_4 \cdot 2H_2O$) in the aerosols was observed in the finer particles that also contained Zn sulfate ($ZnSO_4 \cdot 7H_2O$). On the other hand, the Zn species in the coarser particles were Zn chloride ($ZnCl_2 \cdot 2H_2O$), Zn carbonate ($ZnCO_3$), and Zn sulfide (ZnS), the details of which, including the sources of these species in the coarser particles, will be described elsewhere. In this study, the variation of Zn species from finer to coarser particle size is important, because the effect of oxalate formation should be more marked in the finer particle sizes. Zinc oxalate was not needed to fit the spectra of the coarser particles, but was essential to fit the XANES spectra of the finer particles.

Figure 8 and Table 4 show the fitting of the EXAFS data in k space and the Zn speciation data, respectively. The fitting results of the EXAFS data are more reliable than that of the XANES data, because EXAFS spectra are dependent on the neighboring atoms, interatomic distances, and coordination number, which are sensitive to the Zn speciation. The ratio of Zn oxalate to total Zn species (= [Zn oxalate]/[Zn]total) obtained from the XANES and EXAFS fitting were similar (Tables 3 and 4, Fig. S6), which suggests the presence of Zn oxalate, particularly in the finer particle region. Moreover, the [Zn oxalate]/[Zn]total ratio in each period clearly increased with decreasing particle size (Tables 3 and 4, Fig. S6). This result

shows that Zn oxalate was mainly formed in the aqueous phase at the particle surface, which is caused by the increase in [surface area]/[volume] ratio with decreasing particle size, though heterogeneous uptake on aerosol particles cannot be ruled out. This result corresponds to the scanning transmission X-ray microscopy data, which suggests that the formation of organic aerosols in Asian aerosols occurs at the particle surface (Maria et al., 2004), and Russell et al. (2002) also detected carboxylic acids as particle coatings. In addition, the increase in the fraction of Zn oxalate may reflect that the concentration of free oxalate was higher in the finer particles, because the concentrations of Ca^{2+} and Mg^{2+} ions (= competitive ions) decreases with decreasing particle size. This means that free oxalate in the finer particles can react with Zn^{2+} ions.

3.5 Noncomplexed and metal-complexed oxalate species in the aerosols

In this section, the ratio of metal oxalate complexes to total oxalate or noncomplexed oxalate species will be discussed. For this purpose, the concentration of Ca and Zn oxalates were determined by multiplying: (a) the total concentration of Zn and Ca obtained from ICP-AES data, and (b) the oxalate complex fractions of these ions obtained from XAFS data. On the other hand, the concentration of total oxalate (i.e., the sum of noncomplexed and metal complexed oxalate species) was quantified using IC. The total concentration of oxalate, Ca, and Zn could be obtained using this method despite the low solubility of Ca and Zn oxalate complexes in the water extraction procedure, because these complexes were completely dissolved in our experiments, as we added an excess of water in the water-extraction procedure. For example, the total weight of the aerosols (in the 1/8 cut filter) was <1 mg, or the Ca oxalate on the filter was <0.025 mg assuming that the Ca in the sample was 5 wt% and the fraction of Ca oxalate among the total Ca was 50 mol%. Note that the concentration of Ca and the fraction of Ca oxalate assumed in the calculations were larger than the values measured in our samples. On the other hand, the solubility data (Table 1) showed that the amount of Ca oxalate that could be dissolved in 5 mL of the MQ water employed in this study was 0.035 mg, which was larger than the 0.025 mg. Thus, the Ca oxalate in the aerosols could be completely dissolved in 5 mL water in our experiments. A similar case can be discussed to validate the Zn oxalate data. Thus, we can obtain the concentrations of the total oxalate, Ca, and Zn in the samples using our water extraction procedure.

The $\{[Zn\ oxalate]+[Ca\ oxalate]\}/[oxalate]_{total}$ ratio, determined as described above, is important to evaluate whether or not oxalate species contribute to the increase of hygroscopicity of aerosols. As discussed in the introduction and in Sec. 3.3, noncomplexed oxalic acid in aerosols can contribute to enhancement of the CCN activity and can have a cloud lifetime effect (Pang et al., 2001; Grahan et al., 2004; Kanakidou et al., 2005; Lohmann and Leck, 2005; IPCC, 2007; Chan et al., 2008; Hallquist et al., 2009; Sullivan et al., 2009), whereas Ca and Zn oxalates do not have this potential because of their low hygroscopic and insoluble natures (Table 1). In winter, Ca and Zn oxalates accounted for about 60% of the total oxalate in the size ranges 1.1–2.1 μm and 0.65–1.1 μm, while the values were 60–80% in the summer (Fig. 9). The sum of the Ca and Zn oxalate fractions in the 0.43–0.65 μm range among the total oxalate concentration was approximately 30% in both periods (Fig. 9). The fraction of Zn oxalate among the total oxalate concentration under 0.43 μm in winter was low, while that in summer was very high (Fig. 9). Calcium oxalate in the 2.1–3.3 μm range in summer could not be detected because of the low [oxalate]/[Ca] ratio.

Similar to the case of Ca and Zn oxalates, it is possible that other metal oxalate complexes are present in the aerosols. The size distribution of Mg in the aerosols was similar to that of Ca. The concentration of Mg was approximately 10–90% and 10–20% of Ca in the summer and winter, respectively (Table S3). Although Mg oxalate is more soluble than Ca oxalate, it is much less soluble than K and Na oxalates. Thus, it is possible that complexation with Mg also contributes to make oxalate species more insoluble or less hygroscopic than noncomplexed

oxalate species. Other metal oxalate species, such as with Pb^{2+} and Cu^{2+} ions supplied from anthropogenic sources, can be formed considering their high stability constants with oxalate ions (Table 1) in finer particle size ranges. Some other metal ions that were not measured may also form metal oxalate complexes in this particle range, because some anthropogenic metals in the aerosols are usually rich in finer particles (e.g., Espinosa et al., 2001; Manoli et al., 2002; Hao et al., 2007).

In summary, considering Ca^{2+}, Zn^{2+}, and other metal ions in the aerosols and the formation of their metal oxalate complexes, most of the oxalate in the aerosols can exist as metal oxalate complexes, but not as noncomplexed oxalate species. Thus, it is possible that oxalic acid in the aerosols cannot contribute to the increase of the CCN activity in the atmosphere. These results indicate that any other dicarboxylic acids, such as malonic and succinic acids, can also form metal complexes in aerosols because of their high stability. These may absorb a lesser amount of water than noncomplexed acids, which suggests that a reevaluation of the indirect cooling effect originated from dicarboxylic acids in aerosols is required.

3.6 Implications for oxalate species in the aerosols

The size distribution of oxalate reflects the possible formation pathways of oxalate in aerosols: (i) particulate oxalate formed by gas to particle conversion captured by preexisting aerosols, (ii) oxalate formed in an aqueous phase on the particle surface, and (iii) oxalate formed by reactions in in-cloud processes, (iiii) oxalate can be formed by the photooxidation process. Previous studies have supported that a chemical reaction in an aqueous phase, such as in-cloud or on a particle surface, leads to the formation of oxalate (Warneck, 2003; Grahan et al., 2004; Lim et al., 2005; Carltona et al., 2007). If oxalate ions are dissolved in an aqueous phase with other metal ions, then metal oxalate complexes can precipitate depending on the solubility of each complex. For example, cloud water contains oxalate, Ca^{2+}, Na^{+}, and Mg^{2+} ions (Löflunda et al., 2002). In this case, Ca and Mg oxalates would precipitate, but Na oxalate would not; this would be controlled by their solubility (Table 1). Similarly, NH_4^{+} ions are also present in an aqueous phase on the particle surface and in-cloud droplets, but ammonium oxalate ($(NH_4)_2C_2O_4$) does not precipitate because of its highly soluble nature and the low stability constant of the complex.

In our XAFS study, Ca oxalate was found in the droplet mode, suggesting that Ca oxalate in this particle range formed by evaporation of cloud droplets (in-cloud process). When cloud droplets evaporate, the low solubility species precipitate preferentially with the evaporation of the water. In addition, there is also a possibility that oxalate complex is formed in an aqueous phase on the particle surface, as has been suggested for Zn. The distinct difference between Ca and Zn lies in their source, natural and anthropogenic, respectively. Being different from Zn, which is distributed in the finer fractions, Ca is chiefly supplied as mineral dust and/or sea salt in the form of calcite and gypsum, mainly in the coarser particles (Takahashi et al., 2009). As a consequence, the abundance of Ca in the finer region is relatively low. However, if Ca is present as small particles of minerals in the finer particle size region, then it is likely that oxalic acid can dissolve Ca^{2+} ions out of these Ca minerals to form Ca oxalate on the particle surface. This mechanism can explain the shift in the oxalate peak in the size distribution to larger sizes in summer, because the abundance of Ca in the coarser particle size range is larger in the summer.

Zinc oxalate can be the main oxalate species considering its high concentration in aerosols and the large stability constant of the oxalate. In our XAFS study, the [Zn-oxalate]/[Zn]total ratio increased with the decreasing particle size, suggesting that Zn oxalate was rich at the particle surface. Thus, the fraction of Zn oxalate among the total Zn concentration depends on the surface condition of the particulate Zn and the concentration of other competing ions, such as Mg^{2+} or Ca^{2+}.

The speciation of oxalate depends on the concentrations of various metal ions. For example, in a remote marine atmosphere, Ca and Mg oxalates can become the main metal oxalate species in aerosols because: (i) a remote marine atmosphere is not affected by air pollution without heavy metal ions, such as Zn^{2+}, Pb^{2+}, and Cu^{2+}, which have high stability constants with oxalate (Table 1); (ii) free oxalate is produced in a marine atmosphere by photochemical oxidation of precursor organic compounds (Kawamura and Sakaguchi, 1999; Warneck, 2003); and (iii) Ca^{2+} and Mg^{2+} ions are abundant in sea salts. On the other hand, in an atmosphere containing anthropogenic compounds, Zn oxalate can be the main species, because the concentration of Zn^{2+} ions is high and its complex with oxalate is stable.

4 Conclusions

In our study using XAFS spectroscopy, the fraction of the sum of Ca and Zn oxalate complexes among the total oxalate concentration was 20–80%. Considering the presence of other metal ions, such as Mg^{2+}, Pb^{2+}, and Cu^{2+}, the concentration of free oxalic acid can be much lower than that expected. Therefore, the contribution of oxalic acid to hygroscopicity of aerosol particles must have been overestimated. Thus, the present study may claim reevaluation of the potential of oxalic acid to increase the CCN activity of aerosols, because most of the oxalic acid in the aerosols can exist as metal oxalate complexes. Similar to oxalic acid, other WSOCs, such as malonic and succinic acids, can transform to metal complexes in aerosols. Therefore, in discussing the hygroscopicity and related effects of organic aerosols, it is necessary to evaluate the contribution of the complexation of dicarboxylic acids with metal ions.

Acknowledgements.
We are grateful to H. Kamioka, Y. Kanai, S. Yabuki, and A. Ohta for collecting the aerosol samples in the ADEC project. This research was supported by a Grant-in-Aid for Scientific Research in Priority Areas, “Western Pacific Air–Sea Interaction Study (W-PASS)”. This work was performed with the approval of KEK-PF (2007G669 and 2008G683) and SPring-8 (2009B1383 and 2010A1452). This research is a contribution to the Surface Ocean Lower Atmosphere Study (SOLAS).

References

Adachi, K. and Tainosho, Y.: Characterization of heavy metal particles embedded in tire dust, Environ. Int., 30, 1009–1017, 2004.

Bruland, K.W., and Lohan, M.C.: Controls of Trace Metals in Seawater, The Oceans and Marine Geochemistry, 6, Treatise on Geochemistry, Elsevier Ltd, 2003

Buseck, P. R., and Pósfai, M.: Airborne minerals and related aerosol particles: Effects on climate and the environment, Proc. Natl. Acad. Sci. USA, 96, 3372–3379, 1999.

Carltona, A. G., Turpinb, B. J., Altieric, K. E., Seitzingerc, S., Reffd, A., Lime, H. J., and Ervensf, B.: Atmospheric oxalic acid and SOA production from glyoxal: Results of aqueous photooxidation experiments, Atmos. Environ., 41, 7588–7602, 2007.

Chan, M. N., Kreidenweis, S. M., and Chan, C. K.: Measurements of the hygroscopic and deliquescence properties of organic compounds of different solubilities in water and their relationship with cloud condensation nuclei activities, Environ. Sci. Technol., 42, 3602-3608, 2008.

Charlson, R. J., Schwartz, S. E., Hales, J. M., Cess, R. D., Coakley, J. A., Hansen Jr., J. E., and Hofmann, D. J.: Climate forcing by anthropogenic aerosols, Science, 255, 423–430, 1992.

Claeys, M., Graham, B., Vas, G., Wang, W., Vermeylen, R., Pashynska, V., Cafmeyer, J.,

Guyon, P., Andreae, M. O., Artaxo, P., and Maenhaut, W.: Formation of secondary organic aerosols through photooxidation of isoprene, Science, 303, 1173–1176, 2004.
Clegg, N. A. and Toumi, R.: Non-sea-salt-sulphate formation in sea-salt aerosol, J. Geophys. Res., 103, 31095–31102, 1998.
Councell, T., Duckenfield, K., Landa, E., and Callender, E.: Tire-wear particles as a source of zinc to the environment, Environ. Sci. Technol., 38, 4206–4214, 2004.
David, R. L.: Handbook of Chemistry and Physics, 75th Edition, CRC Press, Inc., USA, 1994.
Draxler, R. R. and Rolph, G. D.: HYSPLIT (HYbrid Single-Particle Lagrangian Integrated Trajectory)Model access via NOAA ARL READY Website. http:// www.arl.noaa.gov/ready/hysplit4. html, NOAA Air Resources Laboratory, Silver Spring, MD, USA. 2003.
Decesari, S., Facchini, M. C., Fuzzi, S., and Tagliavini, E.: Characterization of water soluble organic compounds in atmospheric aerosol: A new approach, J. Geophys. Res., 105, 1481–1489, 2000.
Espinosa, A. J. F., Rodr´ıguez, M. T., de la Rosa, F. J. B., and S´anchez, J. C. J.: Size distribution of metals in urban aerosols in Seville (Spain), Atmos. Environ., 35, 2595–2601, 2001.
Ervens, B., and Volkamer, R.: Glyoxal processing by aerosol multiphase chemistry: towards a kinetic modeling framework of secondary organic aerosol formation in aqueous particles, Atmos. Chem. Phys., 10, 8219-8244, 2010.
Grahan, K. K., Hegg, D., Covert, S. D., and Jonsson, H.: An exploration of aqueous oxalic acid production in the coastal marine atmosphere, Atmos. Environ., 38, 3757–3764, 2004.
Hallquist, M., Wenger, 5 J. C., Baltensperger, U., Rudich, Y., Simpson, D., Claeys, M., Dommen, J., Donahue, N. M., George, C., Goldstein, A. H., Hamilton, J. F., Herrmann, H., Hoffmann, T., Iinuma, Y., Jang, M., Jenkin, M. E., Jimenez, J. L., Kiendler-Scharr, A., Maenhaut, W., McFiggans, G., Mentel, Th. F., Monod, A., Prvt, A. S. H., Seinfeld, J. H., Surratt, J. D., Szmigielski, R., and Wildt, J.: The formation, properties and impact of secondary organic aerosol: current and emerging issues, Atmos. Chem. Phys., 9, 5155–5236, 2009.
Hao, Y., Guo, Z., Yang, Z., Fang, M., and Feng, J.: Seasonal variations and sources of various elements in the atmospheric aerosols in Qingdao, China, Atmos. Res., 85, 27–37, 2007.
Higashi, M., and Takahashi, Y.: Detection of S(IV) species in aerosol particles using XANES spectroscopy, Environ. Sci. Technol., 43, 7357–7363, 2009.
IPCC Climate Change 2007: Synthesis Report, the Intergovernmental Panel on Climate Change, Cambridge University Press, UK, 2007.
Kalberer, M., Yu, J., Cocker, D. R., Flagan, R. C., and Seinfeld, J. H.: Aerosol formation in the cyclohexene-ozone system, Environ. Sci. Technol., 34, 4894–4901, 2000.
Kanai, Y., Ohta, A., Kamioka, H., Terashima, S., Imai, N., Matsuhisa, Y., Kanai, M., Shimizu, H., Takahashi, Y., Kai, K., Xu, B., Hayashi, M., and Zhang, R.: Variation of concentrations and physicochemical properties of aeolian dust obtained in east China and Japan from 2001 to 2002, Bull. Geol. Surv. Jpn., 54, 251–267, 2003.
Kanakidou, M., Seinfeld, J. H., Pandis, S. N., Barnes, I., Dentener, F. J., Facchini, M. C., Van Dingenen, R., Ervens, B., Nenes, A., Nielsen, C. J., Swietlicki, E., Putaud, J. P., Balkanski, Y., Fuzzi, S., Horth, J., Moortgat, G. K., Winterhalter, R., Myhre, C. E. L., Tsigaridis, K., Vignati, E., Stephanou, E. G., and Wilson, J.: Organic aerosol and global climate modelling: A review, Atmos. Chem. Phys., 5, 1053–1123, 2005, http://www.atmos-chem-phys.net/5/1053/2005/.
Kaneyasu, N., Yoshikado, H., Mizuno, T., Sakamoto, K., Soufuku, M.: Chemical forms and sources of extremely high nitrate and chloride in winter aerosol pollution in Kanto plain of Japan. Atmos. Environ., 33, 1745–1756, 1999.
Kauppinen, E. I. and Pakkanen, A. T.: Coal combustion aerosols: A field study, Environ. Sci.

Technol., 24, 1811–1818, 1990.
Kawamura, K. and Ikushima, K.: Seasonal changes in the distribution of dicarboxylic acids in the urban atmosphere, Environ. Sci. Technol., 27, 2227–2235, 1993.
Kawamura, K. and Sakaguchi, F.: Molecular distributions of water soluble dicarboxylic acids in marine aerosols over the Pacific Ocean including tropics, J. Geophys. Res., 104, 3501–3509, 1999.
Kawamura, K., Imai, Y., and Barrie, L.: Photochemical production and loss of organic acids in high Arctic 5 aerosols during long-range transport and polar sunrise ozone depletion events, Atmos. Environ., 39, 599–614, 2005.
Kelly, J. T., Chuang, C. C., and Wexler, A. S.: Influence of dust composition on cloud droplet formation, Atmos. Environ., 41, 2904–2916, 2007.
Krueger, B. J., Grassian, V. H., Laskin, A., and Cowin, J. P.: The transformation of solid atmospheric particles into liquid droplets through heterogeneous chemistry: Laboratory insights into the processing of calcium containing mineral dust aerosol in the troposphere, Geophys. Res. Lett., 30, 1148, 2003.
Li, W. J. and Shao, L. Y.: Observation of nitrate coatings on atmospheric mineral dust particles, Atmos. Chem. Phys., 9, 1863–1871, 2009.
Lim, H. J., Carlton, A. G., and Turpin, B. J.: Isoprene forms secondary organic aerosol through cloud processing: Model simulations, Environ. Sci. Technol., 39, 4441–4446, 2005.
Lohmann, U. and Leck, C.: Importance of submicron surface-active organic aerosols for pristine Arctic clouds, Tellus, 57B, 261–268, 2005.
Löflunda, M., Kasper-Giebl, A., Schustera, B., Gieblb, H., Hitzenbergerb, R., and Puxbauma, H.: Formic, acetic, oxalic, malonic and succinic acid concentrations and their contribution to organic carbon in cloud water, Atmos. Environ., 36, 1553–1558, 2002.
Manceau, A., Marcus, M. A., and Tamura, N.: Quantitative speciation of heavy metals in soils and sediments by synchrotron X-ray techniques, Rev. Mineral. Geochem., 49, 341–428, 2002.
Manoli, E., Voutsa, D., and Samara, C.: Chemical characterization and source identification/ apportionment of fine and coarse air particles in Thessaloniki, Greece, Atmos. Environ., 36, 949–961, 2002.
Maria, S. F., Russell, L. M., Gilles, M. K., and Myneni, S. C. B.: Organic aerosol growth mechanisms and their climate-forcing implications, Science, 306, 1921–1924, 2004.
Martell, A. E. and Smith, R. M.: Critical Stability Constants. Volume 3, Other Organic Ligands, Plenum, New York, USA, 1977.
Mikami, M., Shi, G. Y., and Uno, I.: Aeolian dust experiment on climate impact: An overview of Japan-China joint project ADEC, Global Planet. Change, 52, 142–172, 2006.
Mochida, M., Umemoto, N., Kawamura, K., and Uematsu, M.: Bimodal size distribution of C-2-C-4 dicarboxylic acids in the marine aerosols, Geophys. Res. Lett., 30, 1672, 2003.
Mochida, M., Umemoto, N., Kawamura, K., Lim, H. J., and Turpin, B. J.: Bimodal size distributions of various organic acids and fatty acids in the marine atmosphere: Influence of anthropogenic aerosols, Asian dusts, and sea spray off the coast of East Asia, J. Geophys. Res., 112, D15209, 2007.
Moffet, R. C., Desyaterik, Y., Hopkins, R. J., Tivanski, A. V., Gilles, M. K., Wang, Y., Shutthanandan, V., Molina, L. T., Abraham, R. G., Johnson, K. S., Mugica, V., Molina, M. J., Laskin, A., and Prather, K. A.: Characterization of aerosols containing Zn, Pb, and Cl from an industrial region of Mexico City, Environ. Sci. Technol., 42, 7091-7097, 10.1021/es7030483, 2008.
Novakov, T. and Penner, J. E.: Large contribution of organic aerosols to cloud-condensation-nuclei concentrations, Nature, 365, 823–826, 1993.
Ohta, A., Terashima, S., Kanai, Y., Kamioka, H., Imai, N., Matsuhisa, Y., Shimizu, H., Takahashi, Y., Kai, K., Hayashi, M. and Zhang, R.: Grain-size distribution and chemical

composition of water-insoluble components in aeolian dust collected in Japan in spring 2002. Bull. Geol. Surv. Japan 54, 303–322, 2003.
Oum, K. W., Lakin, M. J., DeHaan, D. O., Brauers, T., and Finlayson-Pitts, B. J.: Formation of molecular chlorine from the photolysis of ozone and aqueous sea-salt particles, Science, 279, 74–77, 1998.
Peng, C., Chan, M. N., and Chan, C. K.: The hygroscopic properties of dicarboxylic and multifunctional acids: Measurements and UNIFAC predictions, Environ. Sci. Technol., 35, 4495–4501, 2001.
Rauch, J. N. and Pacyna, J. M.: Earth's global Ag, Al, Cr, Cu, Fe, Ni, Pb, and Zn cycles, Global Biogeochem. Cy., 23, GB2001, 2009.
Ravel, B. and Newville, M.: ATHENA, ARTEMIS, HEPHAESTUS: Data analysis for X-ray absorption spectroscopy using IFEFFIT, J. Synchrotron Rad., 12, 537–541, 2005.
Russell, L. M., Maria, S. F., and Myneni, S. C. B.: Mapping organic coatings on atmospheric particles, Geophys. Res. Lett., 29, Art. No. 1779, 2002.
Satsumbayashi, H., Kurita, H., Yokouchi, Y., and Ueda, H.: Mono and dicarboxylic acids under long-range transport of air pollution in Japan, Tellus 41B, 219–229, 1989.
Satsumbayashi, H., Kurita, H., Yokouchi, Y., and Ueda, H.: Photochemical formation of particulate dicarboxylic acids under long-range transport in Japan, Atmos. Environ., 24A, 1443–20 1450, 1990.
Saxena, P. and Hildemann, L. M.: Water soluble organics in atmospheric particles: A critical review of the literature and application of thermodynamics to identify candidate compounds, J. Atmos. Chem., 24, 57–109, 1996.
Seinfeld, J. H. and Pandis, S. N.: Atmospheric Chemistry and Physics: From Air Pollution to Climate Change, Second Edition, John Wiley and Sons, NY, USA, 2006.
Sempéré, R., and Kawamura, K.: Low molecular weight dicarboxylic acids and related polar compounds in the remote marine rain samples collected from Western Pacific, Atmos. Environ., 30, 1609–1619, 1996.
Sullivan, R. C. and Prather, K. A.: Investigations of the diurnal cycle and mixing state of oxalic acid in individual particles in Asian aerosol outflow, Environ. Sci. Technol., 41, 8062–8069, 2007.
Sullivan, R. C., Moore, M. J. K., Petters, M. D., Kreidenweis, S. M., Roberts, G. C., and Prather, K. A.: Effect of chemical mixing state on the hygroscopicity and cloud nucleation properties of calcium mineral dust particles, Atmos. Chem. Phys., 9, 3303–3316, 2009.
Takahashi, Y., Kanai, Y., Kamioka, H., Ohta, A., Maruyama, H., Song, Z., and Shimizu, H.: Speciation of sulfate in size-fractionated aerosol particles using sulfur K-edge X-ray absorption near-edge structure, Environ. Sci. Technol., 40, 5052–5057, 2006.
Takahashi, Y., Miyoshi, T., Higashi, M., Kamioka, H., and Kanai, Y.: Observation of transformation of calcite to gypsum in mineral aerosols by Ca K-edge X-ray absorption near-edge structure (XANES), Atoms. Environ., 42, 6535–6541, 2008.
Takahashi, Y., Miyoshi, T., Higashi, M., Kamioka, H., and Kanai, Y.: Neutralization of calcite in mineral aerosols by acidic sulfur species collected in China and Japan studied by Ca K-edge X-ray Absorption Near-Edge Structure, Environ. Sci. Technol., 43, 6535–6540, 2009.
Thornton, J. A., Kercher, J. P., Riedel, T. P., Wagner, N. L., Cozic, J., Holloway, J. S., Dube, W. P., Wolfe, G. M., Quinn, P. K., Middlebrook, A. M., Alexander, B., and Brown, S. S.: A large atomic chlorine source inferred from mid-continental reactive nitrogen chemistry, Nature, 464, 271–274, 2010.
Tsigaridis, K. and Kanakidou, M.: Secondary organic aerosol importance in the future atmosphere, Atmos. Environ., 41, 4682–4692, 2007.
Turpin, B. J., Saxena, P., and Andrews, E.: Measuring and simulating particulate organics in the atmosphere: Problems and prospects, Atmos. Environ., 34, 2983–3013, 2000.
Uematsu, M., Hattori, H., Nakamura, T., Narita, Y., Jung, J., Matsumoto, K., Nakaguchi, Y.,

Kumar, M. D.: Atmospheric transport and deposition of anthropogenic substances from the Asia to the East China Sea, Mar. Chem., 120, 108–115, 2010.
Var, F., Narita, Y., and Tanaka, S.: The concentration trend and seasonal variation of metals in the atmosphere in 16 Japanese cities shown by the results of National Air Surveillance Network (NASN) from 1974 to 1996, Atmos. Environ., 34, 2755–2770, 2000.
Warneck, P.: In-cloud chemistry opens pathway to the formation of oxalic acid in the marine atmosphere, Atmos. Environ., 37, 2423–2427, 2003.
Yao, X., Fang, M., and Chan, C. K.: Size distributions and formation of dicarboxylic acids in atmospheric particles, Atmos. Environ., 36, 2099–2107, 2002.
Yao, X., Fang, M., and Chan, C. K.: The size dependence of chloride depletion in fine and coarse sea-salt particles, Atmos. Environ., 37, 743–751, 2003.
Zappoli, S., Andracchio, A., Fuzzi, S., Facchini, M. C. A., Gelencsér, A., Kiss, G., Krivácsy, Z., Molnár, A., M´eszáros, E., Hansson, H. C., Rosman, K., and Zebühr, Y.: Inorganic, organic and macromolecular components of fine aerosol in different areas of Europe in relation to their water solubility, Atmos. Environ., 33, 2733–2743, 1999.
Zhuang, H., Chan, C. K., Fang, M., and Wexler, A. S.: Formation of nitrate and non-sea-salt sulfate on coarse particles, Atmos. Environ., 33, 4223–4233, 1999.

Figure captions

Fig. 1. The size distribution of the aerosol mass during winter (January 21 to February 12, 2002) and summer (July 28 to August 13, 2002) at Tsukuba, Japan.

Fig. 2. The size distribution of WSCs in aerosols in winter at Tsukuba: (a) anions and (b) cations.

Fig. 3. The size distribution of WSCs in aerosols in summer at Tsukuba: (a) anions and (b) cations.

Fig. 4. The size distribution of Zn in aerosols during winter and summer at Tsukuba.

Fig. 5. Calcium K-edge XANES spectra (open circles = samples, lines = fitting) of finer particles during winter and summer at Tsukuba with those of the standard materials used for fitting.

Fig. 6. The experimental hygroscopic properties of oxalic acid and a Ca oxalate complex.

Fig. 7. Zinc K-edge XANES spectra (open circles = samples, lines = fitting) of finer particles during winter and summer at Tsukuba with those of the standard materials used for fitting.

Fig. 8. Zinc K-edge EXAFS spectra (open circles = sample, lines = fitting) of finer particles during winter and summer at Tsukuba with standard materials used for fitting: (a) 2.1–1.1, 1.1–0.65, and 0.65–0.43 μm in winter, and 2.1–1.1 and 0.65–0.43 μm in summer, and (b) 3.3–2.1 μm in winter and summer.

Fig. 9. Atmospheric concentrations of Ca oxalate, Zn oxalate, and total oxalate during winter and summer.

Table 1. Stability constant (log K) of oxalate with some metal ions at 25 °C (Martell and Smith, 1977) and the solubility of the complexes in water (David, 1994).

	Stability constant (T = 25 °C)		Solubility
	I = 0.10 M	I = 0 M	mg/100 g
K^+	n.d.	–0.80	33000*
Na^+	n.d.	n.d.	6300
Mg^{2+}	2.76	3.43	70
Ca^{2+}	n.d.	3.00	0.67
Cu^{2+}	4.84	6.23	2.53
Zn^{2+}	3.88	4.87	0.79
Pb^{2+}	4.00	4.91	0.16

n.d. : no data;

* : solubility in hot water;

I : ionic strength (M) .

Table 2. Fraction of various Ca species at Tsukuba in winter and summer determined by XANES fitting (mol%).

Season	Particle diameter (μm)	Calcite	Gypsum	Ca oxalate	Ca nitrate	Anhydrite
Winter	> 11	31% ± 2%	38% ± 4%			31% ± 4%
	11–7.0	28% ± 1%	40% ± 3%			32% ± 3%
	7.0–4.7	19% ± 1%	47% ± 3%			34% ± 3%
	4.7–3.3	23% ± 1%	61% ± 3%			16% ± 3%
	3.3–2.1		85% ± 0%			15% ± 0%
	2.1–1.1		56% ± 4%	30% ± 3%	14% ± 2%	
	1.1–0.65		58% ± 3%	20% ± 4%	22% ± 2%	
	0.65–0.43		37% ± 3%	63% ± 3%		
Summer	> 11	18% ± 1%	23% ± 3%			59% ± 3%
	11–7.0		50% ± 3%			50% ± 3%
	7.0–4.7		71% ± 3%			29% ± 3%
	4.7–3.3		71% ± 3%			29% ± 3%
	3.3–2.1		67% ± 4%			33% ± 4%
	2.1–1.1		63% ± 3%	11% ± 2%	26% ± 2%	
	1.1–0.65		54% ± 1%	40% ± 2%	6% ± 3%	

Table 3. Fraction of various Zn species at Tsukuba in winter and summer determined by XANES fitting (mol%).

Season	Particle diameter (μm)	Zn oxalate	Zn sulfate	Zn chloride	Zn carbonate	Zn sulfide
Winter	> 11			56% ± 2%	44 ± 2%	
	11–7.0			59% ± 4%	41 ± 4%	
	7.0–4.7			44% ± 3%	22 ± 2%	34% ± 3%
	4.7–3.3			58% ± 2%	12 ± 1%	30% ± 3%
	3.3–2.1		39% ± 2%	61% ± 2%		
	2.1–1.1	30% ± 2%	70% ± 2%			
	1.1–0.65	63% ± 4%	37% ± 4%			
	0.65–0.43	81% ± 3%	19% ± 3%			
	< 0.43	83% ± 6%	17% ± 6%			
Summer	> 11			69% ± 2%		31% ± 2%
	11–7.0			72% ± 2%		28% ± 2%
	7.0–4.7			53% ± 3%		47% ± 3%
	4.7–3.3			94% ± 1%		6% ± 1%
	3.3–2.1	20% ± 2%	9% ± 2%	71% ± 1%		
	2.1–1.1	46% ± 2%	54% ± 2%			
	1.1–0.65	58% ± 4%	42% ± 4%			
	0.65–0.43	63% ± 3%	37% ± 3%			
	< 0.43	98% ± 6%	2% ± 6%			

Table 4. Fraction of various Zn species at Tsukuba in the winter and summer determined by EXAFS fitting (mol%).

Season	Particle diameter (μm)	Zn oxalate	Zn sulfate	Zn chloride
Winter	3.3–2.1	2% ± 1%	33% ± 3%	65% ± 2%
	2.1–1.1	28% ± 2%	72% ± 2%	
	1.1–0.65	59% ± 4%	41% ± 4%	
	0.65–0.43	79% ± 4%	21% ± 4%	
Summer	3.3–2.1	26% ± 2%	41% ± 17%	33% ± 15%
	2.1–1.1	38% ± 8%	62% ± 8%	
	0.65–0.43	51% ± 12%	49% ± 12%	

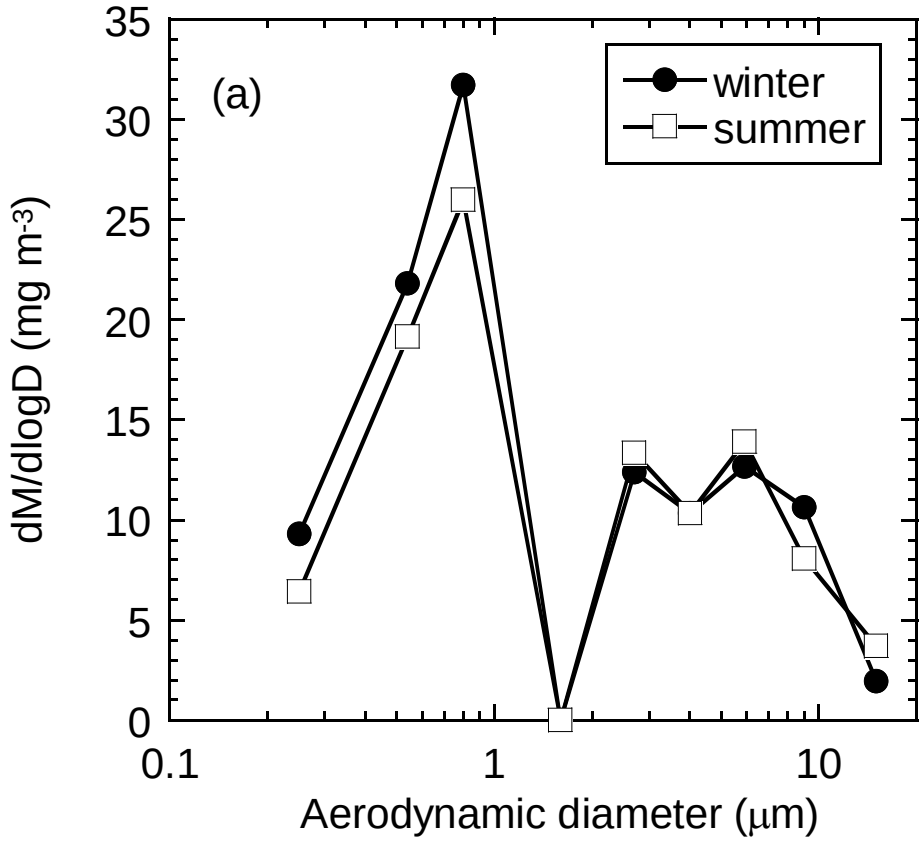
(a)
winter
summer
dM/dlogD (mg m-3)
Aerodynamic diameter (μm)
0
5
10
15
20
25
30
35
0.1
1
10

Fig. 1

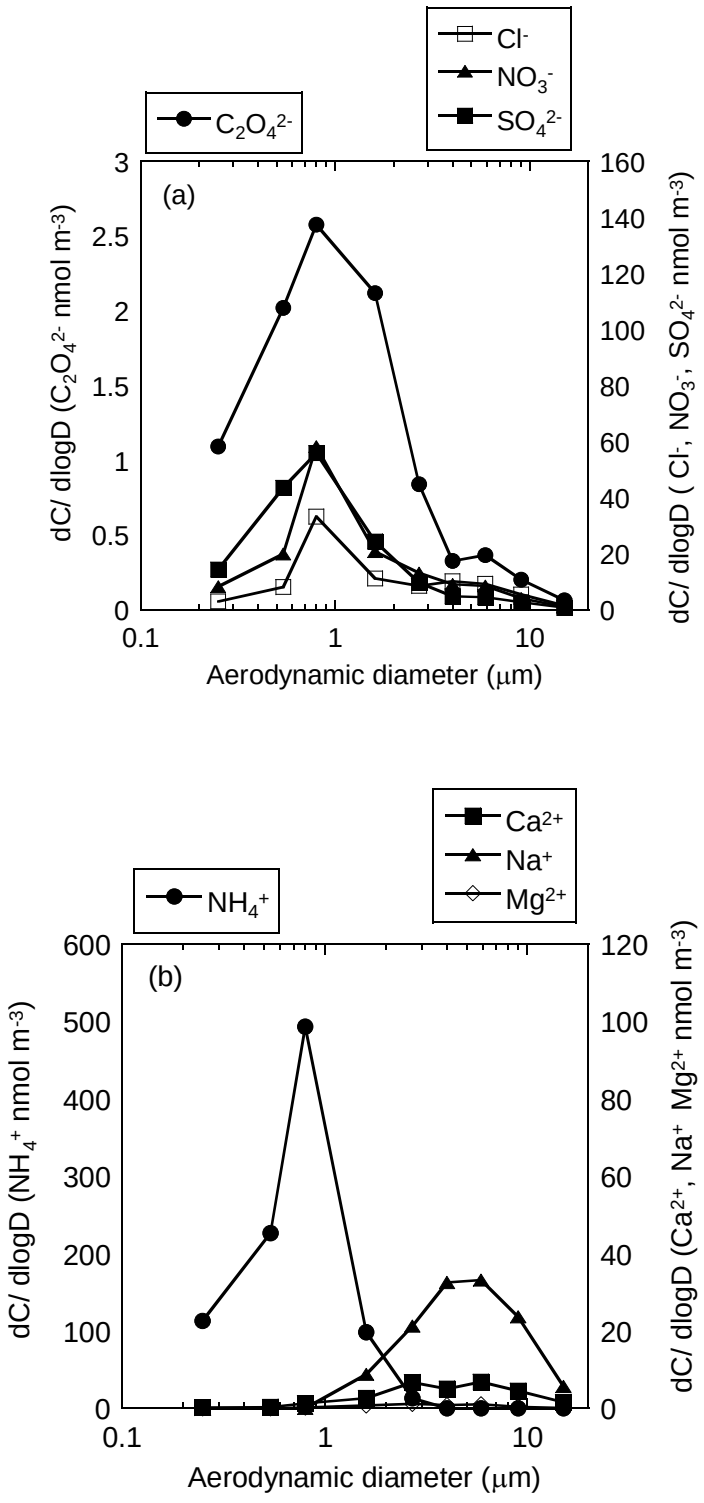
Cl-
NO3-
SO4 2-
C2O4 2-
(a)
dC/ dlogD (C2O4 2- nmol m-3)
dC/ dlogD (Cl-, NO3-, SO4 2- nmol m-3)
Aerodynamic diameter (μm)
Ca2+
Na+
Mg2+
NH4+
(b)
dC/ dlogD (NH4 + nmol m-3)
dC/ dlogD (Ca2+, Na+ Mg2+ nmol m-3)
Aerodynamic diameter (μm)

Fig. 2

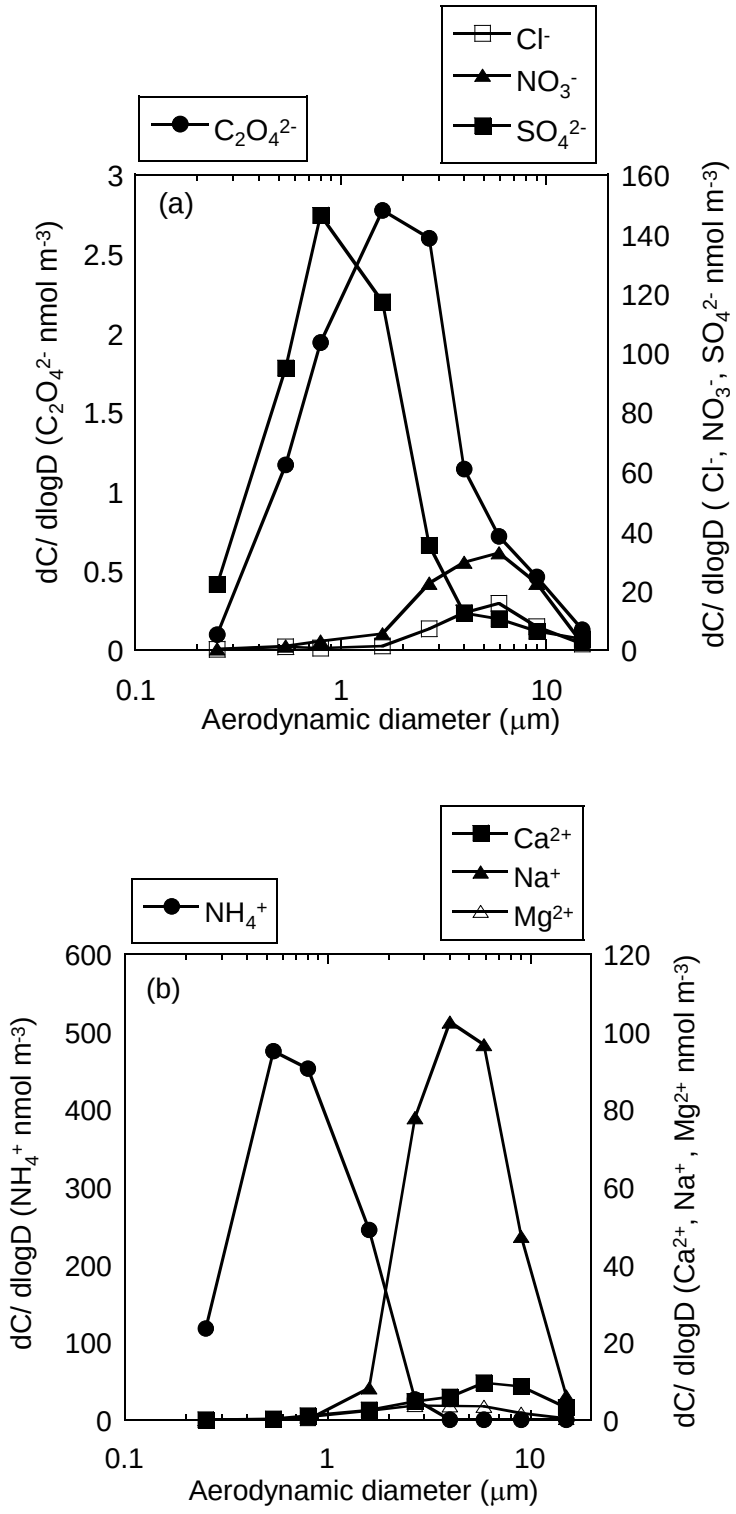
Cl-
NO3-
SO4 2-
C2O4 2-
(a)
dC/ dlogD (C2O4 2- nmol m-3)
dC/ dlogD (Cl-, NO3-, SO4 2- nmol m-3)
Aerodynamic diameter (μm)
Ca2+
Na+
Mg2+
NH4+
(b)
dC/ dlogD (NH4+ nmol m-3)
dC/ dlogD (Ca2+, Na+, Mg2+ nmol m-3)
Aerodynamic diameter (μm)

Fig. 3

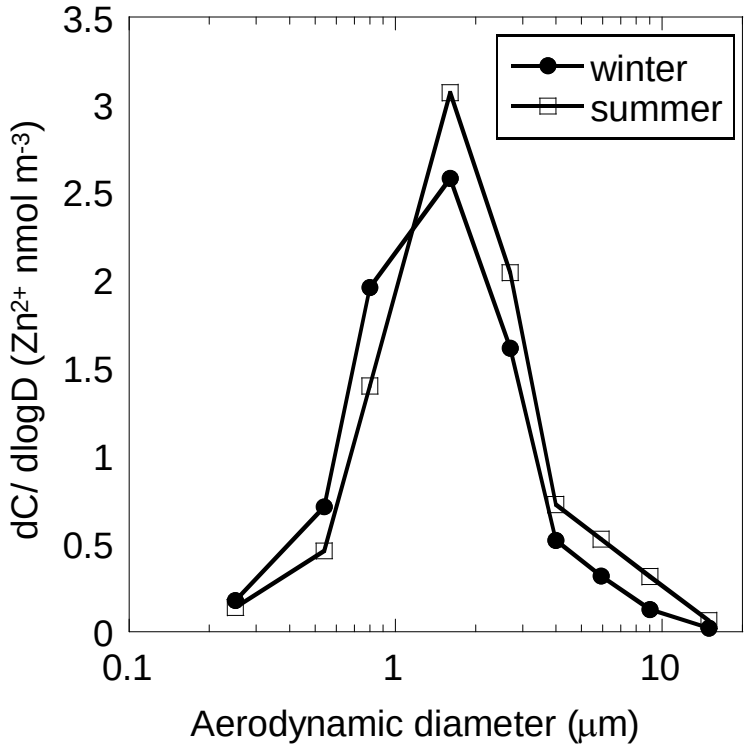
3.5
3
2.5
2
1.5
1
0.5
0
0.1
1
10
dC/ dlogD (Zn2+ nmol m-3)
Aerodynamic diameter (μm)
winter
summer

Fig. 4

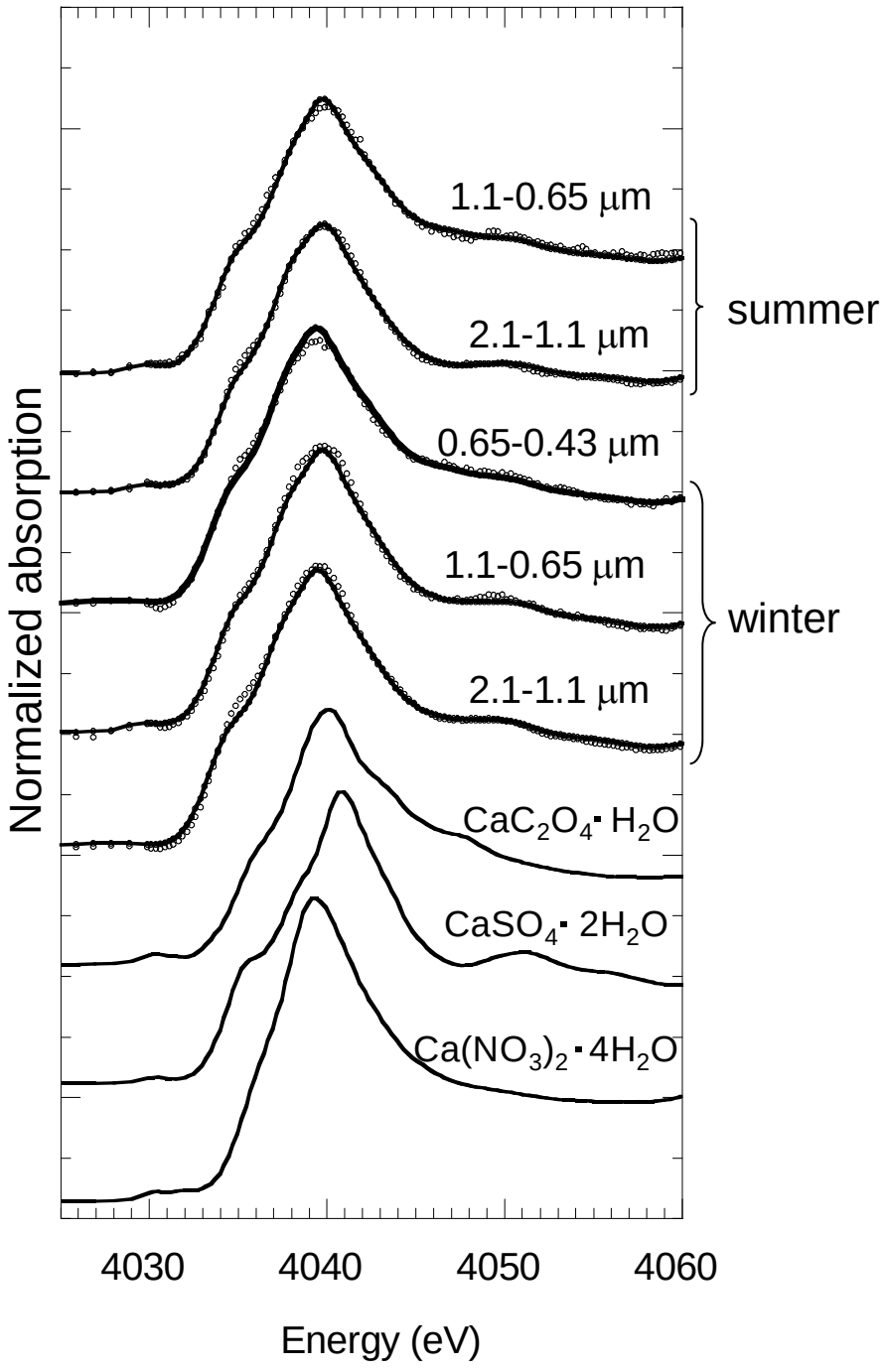
1.1-0.65 μm
2.1-1.1 μm
summer
0.65-0.43 μm
1.1-0.65 μm
2.1-1.1 μm
winter
$CaC_2O_4 \cdot H_2O$
$CaSO_4 \cdot 2H_2O$
$Ca(NO_3)_2 \cdot 4H_2O$
Normalized absorption
4030
4040
4050
4060
Energy (eV)

Fig. 5

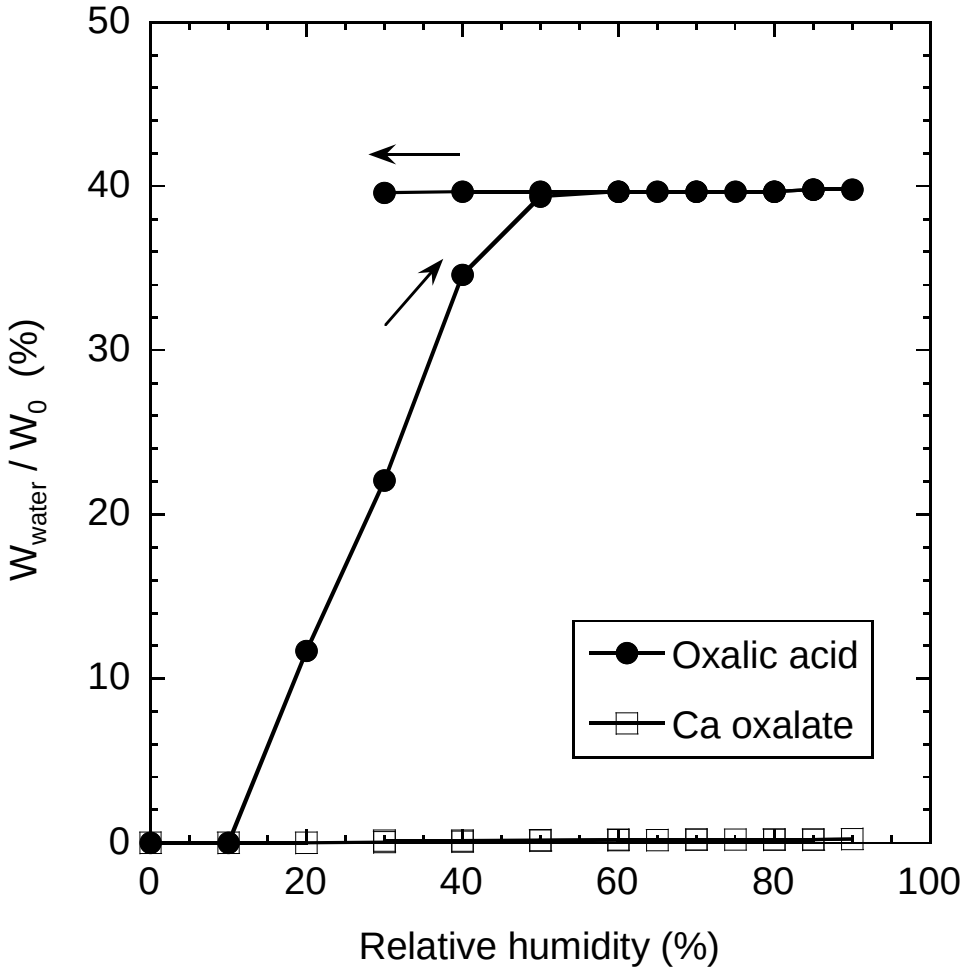
50
40
30
20
10
0
0
20
40
60
80
100
W_{water} / W_0 (%)
Relative humidity (%)
Oxalic acid
Ca oxalate

Fig. 6

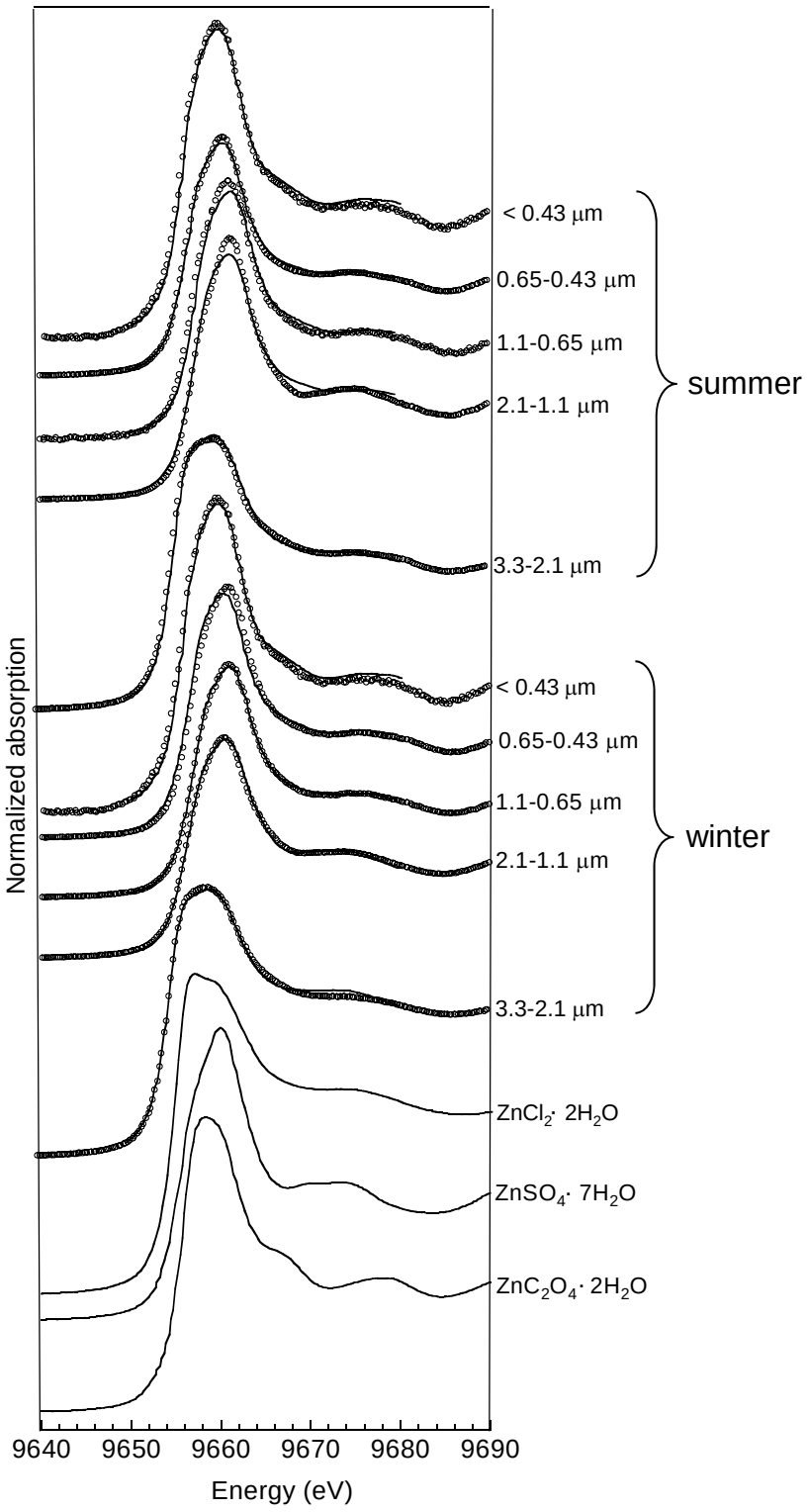
< 0.43 μm
0.65-0.43 μm
1.1-0.65 μm
2.1-1.1 μm
3.3-2.1 μm
summer
< 0.43 μm
0.65-0.43 μm
1.1-0.65 μm
2.1-1.1 μm
3.3-2.1 μm
winter
ZnCl2· 2H2O
ZnSO4· 7H2O
ZnC2O4· 2H2O
Normalized absorption
9640
9650
9660
9670
9680
9690
Energy (eV)

Fig. 7

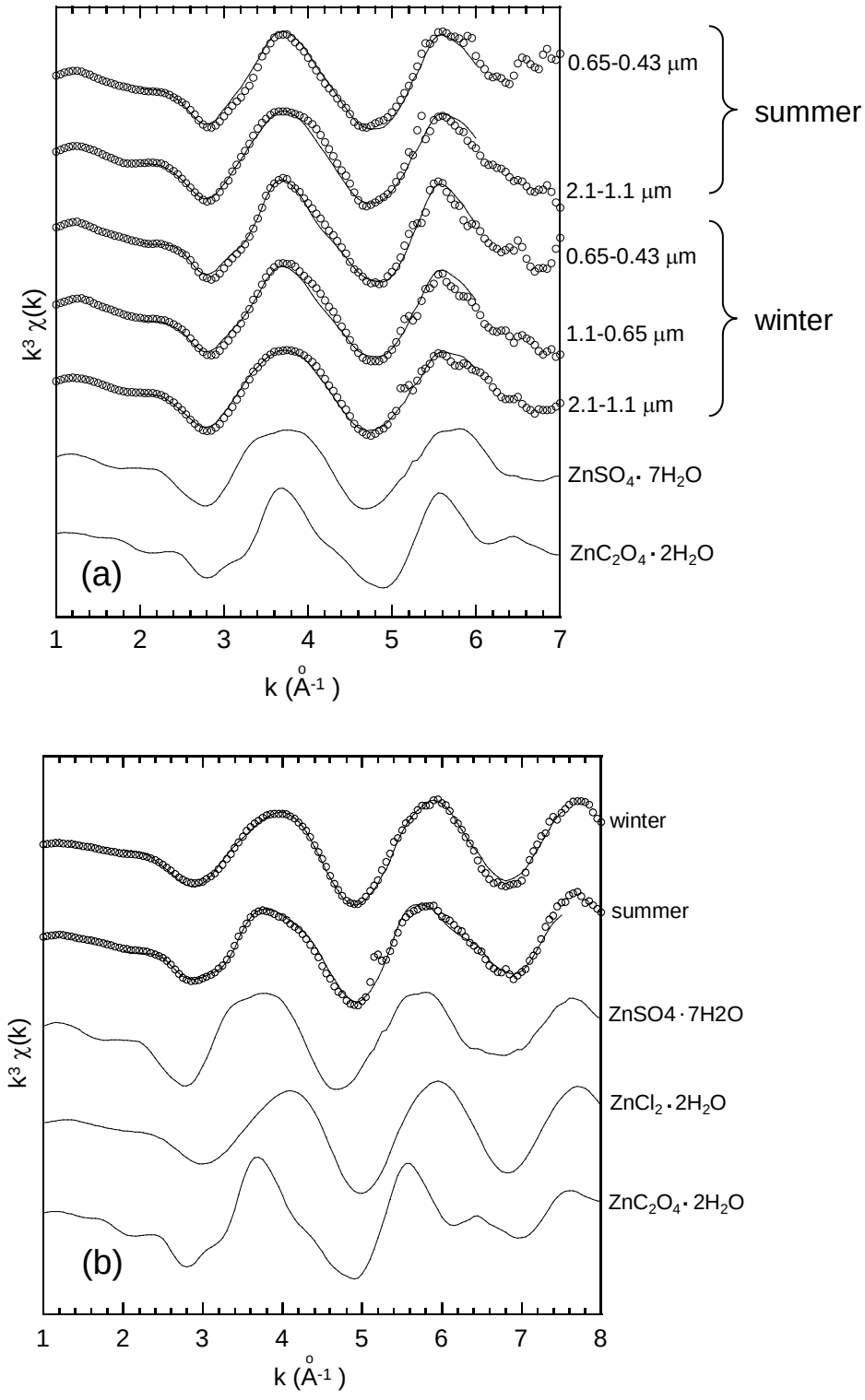
0.65-0.43 μm
2.1-1.1 μm
summer
0.65-0.43 μm
1.1-0.65 μm
2.1-1.1 μm
winter
ZnSO4· 7H2O
ZnC2O4 · 2H2O
(a)
k3 χ(k)
k (Å-1)
winter
summer
ZnSO4 · 7H2O
ZnCl2 · 2H2O
ZnC2O4· 2H2O
(b)
k3 χ(k)
k (Å-1)

Fig. 8

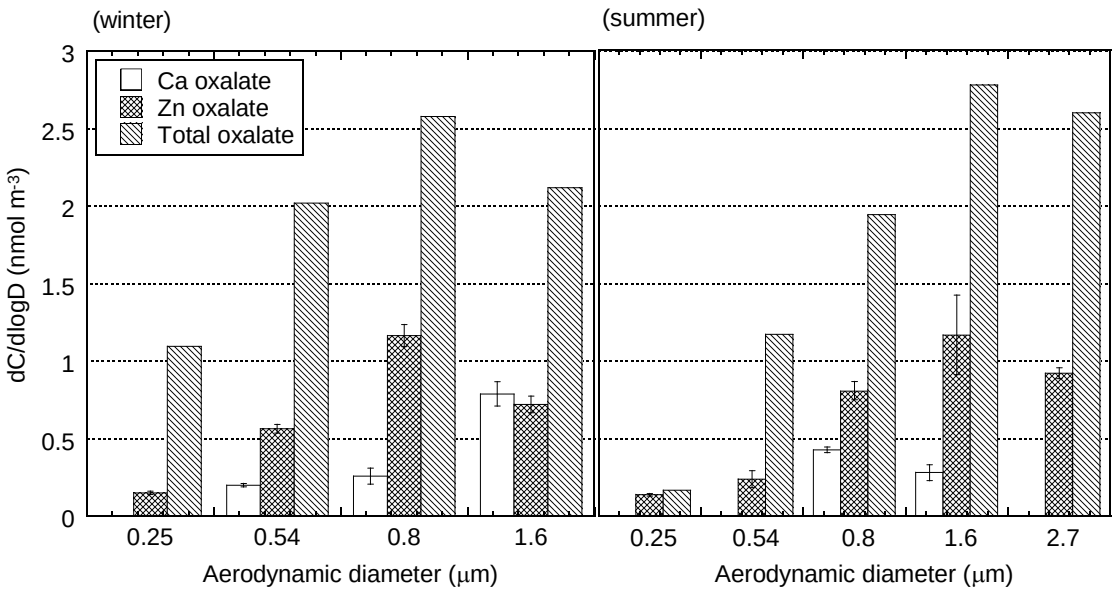
(winter)
(summer)
Ca oxalate
Zn oxalate
Total oxalate
dC/dlogD (nmol m-3)
3
2.5
2
1.5
1
0.5
0
0.25
0.54
0.8
1.6
2.7
Aerodynamic diameter (μm)
Aerodynamic diameter (μm)

Fig. 9

Supporting Materials for

Oxalate metal complexes in aerosol particles: implications for the hygroscopicity of oxalate-containing particles

Takema FURUKAWA and Yoshio TAKAHASHI*

Department of Earth and Planetary Systems Science,

Graduate School of Science, Hiroshima University,

Higashi-Hiroshima, Hiroshima 739-8526, Japan

* Corresponding author

phone: +81-824-24-7460; fax: +81-824-24-0735;

e-mail: ytakaha@hiroshima-u.ac.jp

Table S1. The concentration (nmol/m^3) of non-sea salt sulfate (nss-sulfate) and total sulfate, and the ratio of [nss-sulfate]/[total sulfate] (%) in aerosols in (a) winter and (b) summer.

(a)

winter			
Size (μm)	nss-sulfate	total SO4	nss-sulfate / total SO4
0.25	14.4	14.4	100
0.54	43.5	43.6	100
0.80	55.9	55.9	100
1.6	23.9	24.4	98.2
2.7	8.47	9.56	88.6
4.0	3.03	4.70	64.5
5.9	2.86	4.56	62.7
9.0	1.48	2.69	54.9
15	0.431	0.720	59.8
Total	154	160	96.0

(b)

summer			
Size (μm)	nss-sulfate	total SO4	nss-sulfate /total SO4
0.25	22.0	22.0	100
0.54	95.0	95.0	100
0.80	146	146	100
1.6	117	117	100
2.7	31.3	35.7	88.7
4.0	7.10	12.4	57.5
5.9	5.46	10.4	52.4
9.0	3.96	6.39	62.0
15	3.30	3.62	91.2
total	431	449	96.1

Table S2. The concentration (nmol/m^3) of water soluble components in aerosols (a) winter, (b) summer, and (c) winter/summer.

(a) Winter (January 21 to February 12, 2002)

Size (μm)	Oxalate	Cl^-	NO_3^-	SO_4^{2-}	Ca^{2+}	Na^+	NH_4^+	Mg^{2+}	Zn^{2+}
0.25	1.09	2.91	8.16	14.4	0.160	-	160	-	0.18
0.54	2.02	8.07	19.9	43.6	0.312	-	435	-	0.71
0.8	2.58	33.2	58.2	55.9	1.28	-	767	0.150	1.96
1.6	2.12	11.1	20.8	24.4	2.62	8.75	104	0.680	2.58
2.7	0.840	8.60	13.0	9.56	6.71	21.2	14.0	1.14	1.61
4	0.330	10.2	9.04	4.70	5.03	32.5	-	0.830	0.520
5.9	0.370	9.20	8.57	4.56	6.75	33.2	-	0.990	0.320
9	0.201	5.47	4.05	2.69	4.49	23.7	-	0.420	0.130
15	0.0623	1.41	1.03	0.720	1.55	5.65	-	0.122	0.0200

(b) Summer (July 28 to August 13, 2002)

Size (μm)	Oxalate	Cl^-	NO_3^-	SO_4^{2-}	Ca^{2+}	Na^+	NH_4^+	Mg^{2+}	Zn^{2+}
0.25	0.0983	0.280	0.442	22.03	0.0700	-	118	-	0.140
0.54	1.17	1.11	1.28	95.0	0.270	-	475	-	0.460
0.8	1.94	0.603	3.01	146	1.07	-	453	0.740	1.40
1.6	2.78	1.27	5.44	117	2.55	8.18	245	2.30	3.07
2.7	2.60	7.10	22.5	35.3	4.71	77.9	26.1	3.71	2.04
4	1.14	12.5	29.5	12.4	5.84	103	-	3.60	0.730
5.9	0.720	15.7	32.7	10.4	9.52	96.7	-	3.46	0.530
9	0.460	7.76	22.6	6.39	8.61	47.3	-	1.74	0.310
15	0.130	2.08	2.24	3.62	3.18	6.22	-	0.380	0.0600

(c) Winter / summer

Size (μm)	Oxalate	Cl^-	NO_3^-	SO_4^{2-}	Ca^{2+}	Na^+	NH_4^+	Mg^{2+}	Zn^{2+}
0.25	11.1	10.3	18.5	0.654	2.26	-	1.36	-	1.27
0.54	1.73	7.24	15.5	0.460	1.14	-	0.914	-	1.54
0.8	1.33	55.0	19.3	0.380	1.20	-	1.69	0.200	1.40
1.6	0.763	8.73	3.82	0.208	1.03	1.07	0.425	0.300	0.840
2.7	0.323	1.20	0.580	0.271	1.42	0.273	0.535	0.306	0.790
4	0.290	0.813	0.310	0.380	0.861	0.320	-	0.231	0.720
5.9	0.511	0.590	0.262	0.438	0.708	0.343	-	0.286	0.602
9	0.436	0.705	0.180	0.421	0.522	0.500	-	0.244	0.406
15	0.479	0.681	0.460	0.199	0.487	0.908	-	0.330	0.320

Table S3. Correlation coefficient (R^2) between some ions at various particle diameters.

Winter

	Oxalate	Cl^-	NO_3^-	SO_4^{2-}	Ca^{2+}	Na^+	NH_4^+	Mg^{2+}
Oxalate	1.00							
Cl^-	0.458	1.00						
NO_3^-	0.700	0.920	1.00					
SO_4^{2-}	0.884	0.565	0.796	1.00				
Ca^{2+}	0.282	8.12×10^{-3}	0.0971	0.321	1.00			
Na^+	0.434	0.0370	0.196	0.434	0.850	1.00		
NH_4^+	0.695	0.642	0.831	0.921	0.340	0.425	1.00	
Mg^{2+}	0.113	1.27×10^{-3}	0.0490	0.211	0.884	0.685	0.296	1.00
Zn^{2+}	0.561	0.379	0.445	0.320	1.60×10^{-5}	0.0548	0.168	0.0621

Summer

	Oxalate	Cl^-	NO_3^-	SO_4^{2-}	Ca^{2+}	Na^+	NH_4^+	Mg^{2+}
Oxalate	1.00							
Cl^-	0.0140	1.00						
NO_3^-	4.03×10^{-4}	0.943	1.00					
SO_4^{2-}	0.432	0.333	0.287	1.00				
Ca^{2+}	0.0240	0.791	0.812	0.352	1.00			
Na^+	2.82×10^{-3}	0.913	0.951	0.303	0.650	1.00		
NH_4^+	0.132	0.406	0.418	0.815	0.498	0.427	1.00	
Mg^{2+}	0.183	0.654	0.774	0.0790	0.507	0.814	0.292	1.00
Zn^{2+}	0.899	0.025	6.72×10^{-4}	0.357	0.0160	1.40×10^{-4}	0.0608	0.170

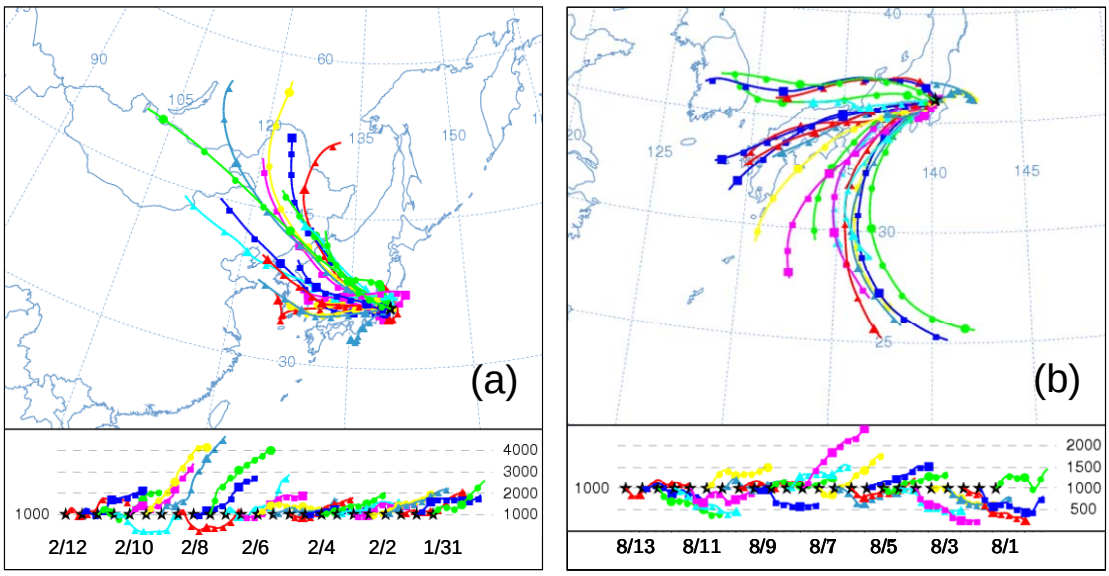

Figure S1. The three dimensional backward trajectory analysis in sampling periods; (a) winter; (b) summer. The NOAA/ARL HYSPLIT model (Draxler and Rolph, 2003) was used for the calculation. The trajectories started at the altitude of 1000 m above the sampling site in Tsukuba.

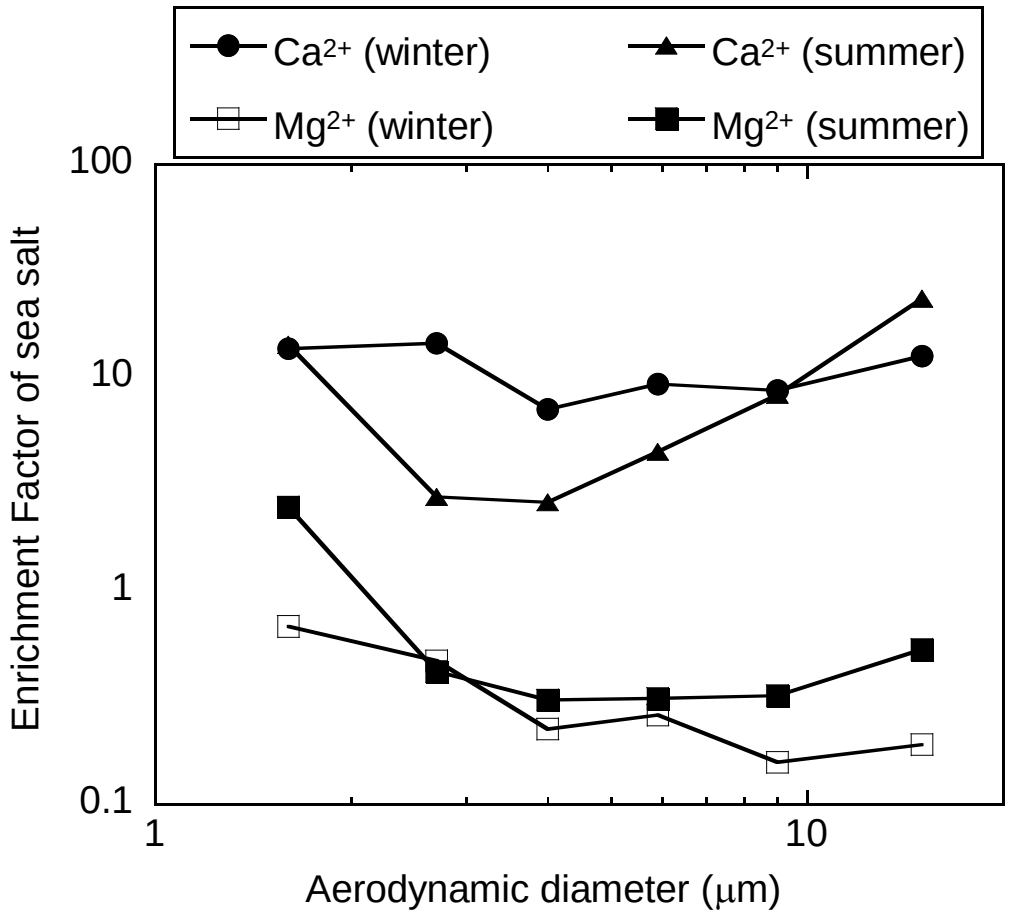

Figure S2. Enrichment factor normalized by sea salt particles for Ca^{2+} and Mg^{2+} in each period.

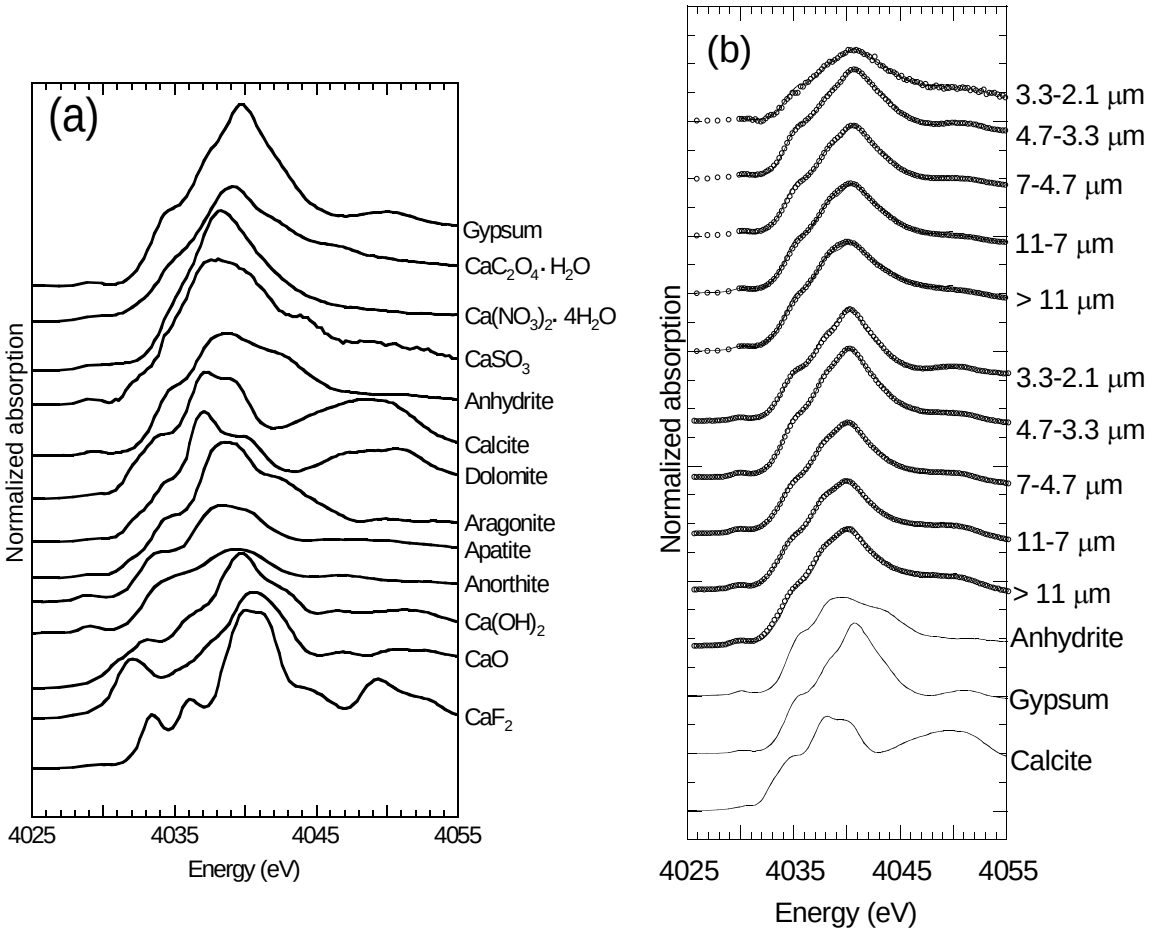

Figure S3. Calcium K-edge XANES; (a) Ca standard materials; (b) coarse particle samples (open circle: samples; lines: fitting) during winter and summer at Tsukuba with standard materials used for fitting.

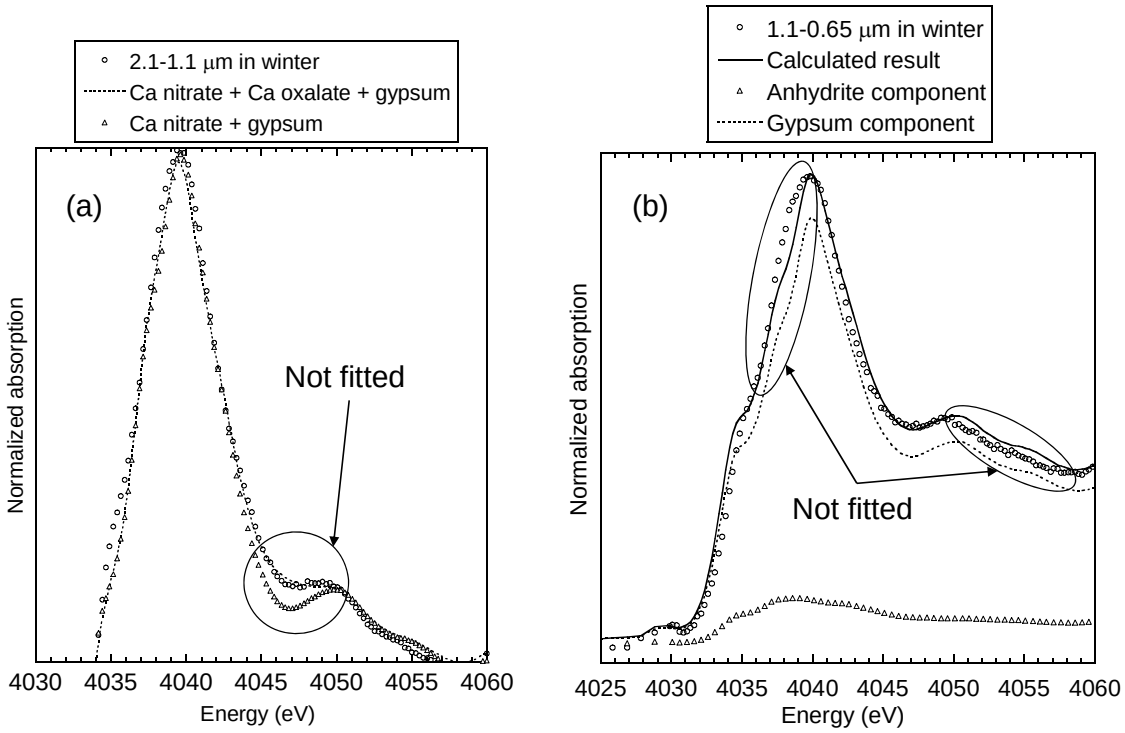

Figure S4. Fitting results of the samples with various standard materials. A circle and ellipses represent the regions of misfit. (a) fitting by Ca nitrate + Ca-oxalate + gypsum (dashed line), Ca nitrate + gypsum (triangle), and 2.1-1.1 μm in winter (circle). (b) fitting result (line) by gypsum (triangle) + anhydrite (triangle) with the spectrum of 1.1-0.65 μm in winter (circle).

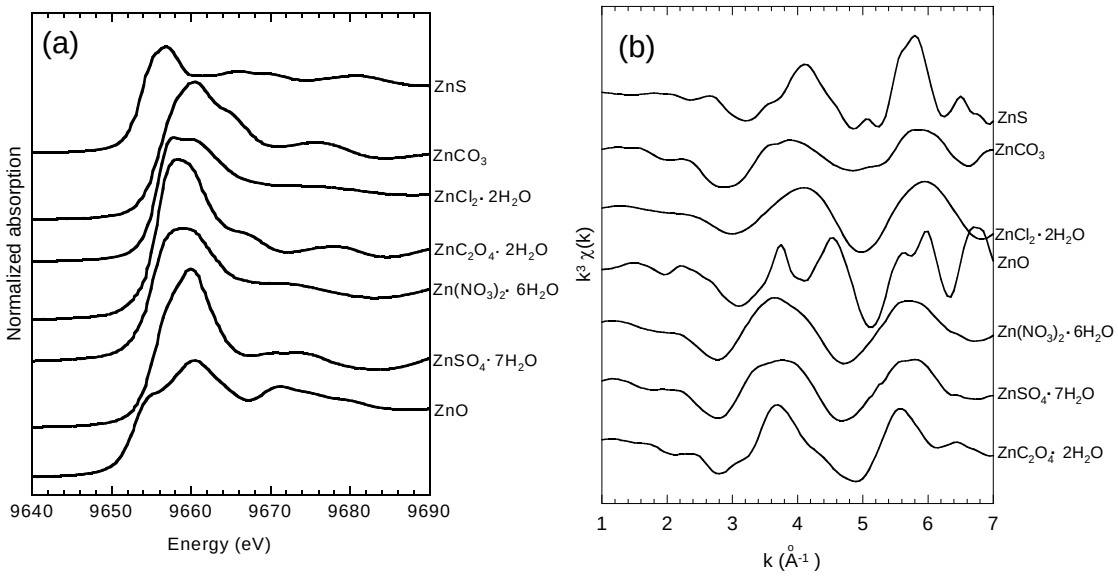

Figure S5. Zinc K-edge XANES (a) and EXAFS (b) for Zn standard materials.

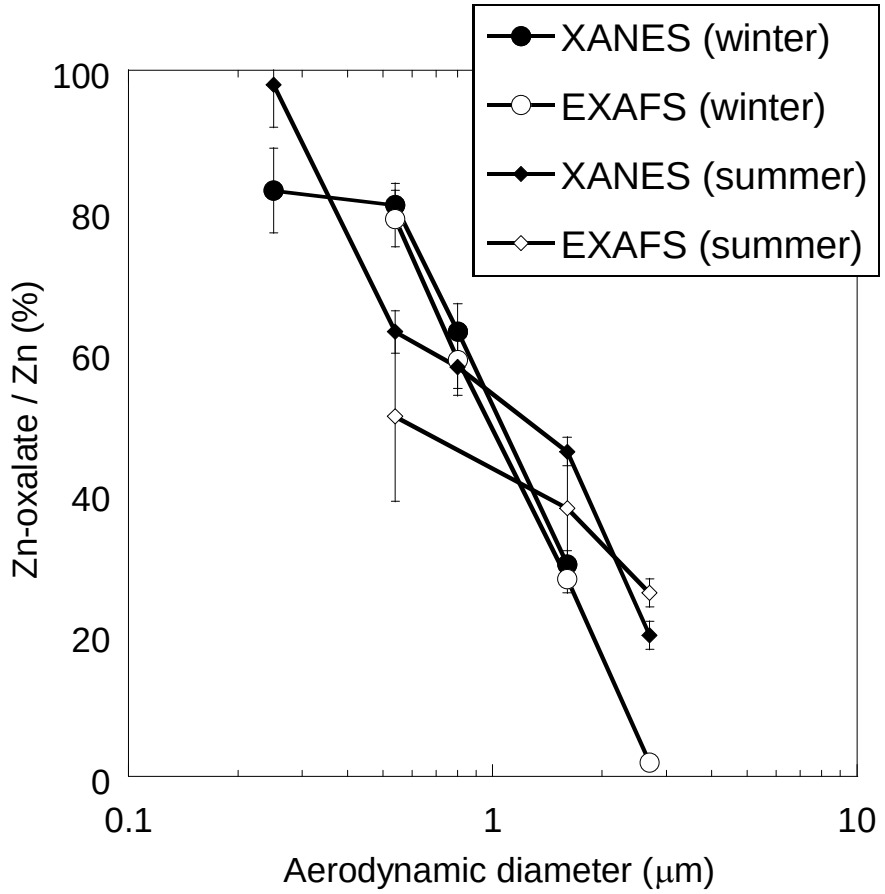

Figure S6. Comparison of the fraction of Zn-oxalate resulting from XANES fitting and EXAFS fitting, which shows the consistency between them.